applied sciences

MDPI

*Article*

# Design of a Bionic Spider Robot with a Two-Degrees-of-Freedom Leg Structure and Body Frame

**Yangwen Nie [1], Daikun Zhu [2,*], Yahui Chen [2], Xing Hu [1] and Liangliang Wang [2]**

[1] Engineering Comprehensive Training Center, Xi'an University of Architecture and Technology, Xi'an 710055, China; yangwennie@xauat.edu.cn (Y.N.); huxing918@163.com (X.H.)
[2] School of Mechanical and Electrical Engineering, Xi'an University of Architecture and Technology, Xi'an 710055, China; chenyahui@xauat.edu.cn (Y.C.); wangliangliang805@xauat.edu.cn (L.W.)
* Correspondence: zhudaikun@xauat.edu.cn; Tel.: +86-152-2915-9003

**Abstract:** Spiders have unique biological characteristics and excellent maneuverability, making them an ideal model for bionic robot design. However, traditional bionic spider robot designs usually have multiple degrees of freedom and confront many challenges. These challenges include complex control requirements, higher energy consumption, larger size and weight, higher risk of failure, and higher cost. This study proposes a leg design with two degrees of freedom to reduce its control and manufacturing costs. It can better control leg movement and improve leg force through a multi-link mechanism and a dual-motor system. In addition, the triangular gait and hexagonal body structure align the weight of the body with the support point, thereby enhancing stability. This study offers a comprehensive and organized approach to bio-inspired robot design, providing a valuable reference for future bionic robot development.

**Keywords:** biomimetic spider robot; two-DOF leg structure design; triangular gait; hexagonal body frame; stability enhancement

check for updates

**Citation:** Nie, Y.; Zhu, D.; Chen, Y.; Hu, X.; Wang, L. Design of a Bionic Spider Robot with a Two-Degrees-of-Freedom Leg Structure and Body Frame. *Appl. Sci.* **2024**, *14*, 9809. https://doi.org/10.3390/app14219809

Academic Editor: Yutaka Ishibashi

Received: 17 September 2024
Revised: 24 October 2024
Accepted: 25 October 2024
Published: 27 October 2024

**Copyright:** © 2024 by the authors. Licensee MDPI, Basel, Switzerland. This article is an open access article distributed under the terms and conditions of the Creative Commons Attribution (CC BY) license (https://creativecommons.org/licenses/by/4.0/).

## 1. Introduction

The inspiration for the biomimetic robots was originally derived from biology, and it was an imitation of biological form and movement [1]. In recent years, biomimetic robots have found extensive applications in the military, industry, and health and environmental protection industries due to the continuous advancement of technology. For example, bionic robots are used for complex environment detection [2–4], disaster relief [5,6] and pipeline detection [7–9]. At present, biomimetic robots have become a research area of concern, mainly focusing on the study of biomimetic structures, materials and control systems. The study of biomimetic structures requires detailed research and analysis on the physiological structure, function and behavior of organisms, with the purpose of integrating the advantages of organisms into mechanical design, such as unmanned aerial vehicles designed using the flight principle of insects [10] and underwater vehicles designed to imitate fish swimming [11]. At the same time, biomimetic materials research focuses on the innovative creation and application of materials, such as bionic skin [12,13], bionic bone [14], and bionic muscle [15,16]. Biomimetic control technology is also a prominent research field, mainly aiming at research on the biological nervous system [17,18] and the research of control methods oriented towards the biological nervous system [19].

Among many bionic objects, spiders are favored by many researchers and have become popular bionic objects because of their unique biological characteristics and outstanding athletic ability. For example, in terms of mechanical structure and control, Marinoni and Bono [20] achieved modeling and control of a quadruped spider robot through simulation and proportional prototyping; Kravchenko et al. [21] proposed a mathematical model for spider robots aimed at group control synthesis, emphasizing the potential for multi robot collaboration and practical applications; Zhu Y et al. [22] studied the omnidirectional

jumping ability of legged robots based on the behavioral mechanism of jumping spiders; Sun C et al. [23] designed and conducted simulation analysis of a hexapod biomimetic spider robot, emphasizing its advantages in flexibility and stability; Liu C et al. [24] proposed a biomimetic design and technological innovation method by studying the hydraulic joints in spider legs and combining biomimetics, computational fluid dynamics (CFD) simulation, and design; Mingyou et al. [25] explored the design and analysis of control systems for spider-like robots, with a focus on their application in maintenance engineering. Finally, Jiang et al. [26] developed a spider joint-shaped biomimetic actuator with an approximate triangular prism shape, demonstrating new potential in robot motion and load-bearing capacity.

In existing research, the leg motion structures of biomimetic spider robots are often designed to incorporate multiple degrees of freedom (DOFs), which simulate the movement capabilities of spiders. Although this can simulate the movement ability of spiders well, it also brings many challenges. First of all, each degree of freedom requires an independent control, and multiple degrees of freedom result in greatly increased complexity of the control, and it is difficult to achieve autonomous operation due to the complexity of the environment [27]. Secondly, the need for additional actuators to drive multi-degree-of-freedom structures can lead to increased energy consumption, especially in environments with limited energy resources [28]. Thirdly, the additional weight and volume required to adapt to multi-degree-of-freedom configurations increase the complexity of manufacturing and maintenance, thereby limiting the applicability of the robot environment. In addition, the increase in the number of components in multi-degree-of-freedom structures increases the likelihood of component failures, which may impair the performance of robots and even lead to system failures. Therefore, although the multi-degree-of-freedom structure design endows biomimetic spider robots with the ability to simulate spider movements well, it poses obstacles to their widespread adoption and development.

This work aims to tackle these problems by specifically examining and analyzing the limb configuration and body frame structure of biomimetic spider robots. Through the utilization of a composite linkage mechanism and the modification of the leg structure, we have successfully developed a two-degree-of-freedom leg design for the biomimetic spider robot. This design not only improves the robot's ability to move and bend but also streamlines the leg muscles and hydraulic systems, resulting in more effective control of leg motion using a dual-motor system. We have implemented a transmission system that modifies the force exerted on the motors, therefore safeguarding the robot against external forces and minimizing energy consumption caused by resisting torques in different directions. Through the comparative analysis of various gaits, the triangular gait and its corresponding hexagonal body structure are selected as the gait and structure of the bionic spider robot. This structure can ensure that the bionic spider robot can align its center of gravity with its support point, ensuring stability during movement, and at the same time, it can prevent excessive weight on one leg. This research provides a comprehensive approach for creating biomimetic robot systems, and will also provide indispensable resources in the future robot design process to simulate biological systems.

The main work completed in this paper is as follows:

(1) A new two-degree-of-freedom bionic spider robot leg mechanism is designed. Compared with the existing structure, it has less control difficulty, lower cost and an optimized force structure.
(2) A body frame selection method is proposed to provide a basis for the selection of bionic spider robot frames with different gaits.
(3) MATLAB R2023a is used to complete leg motion simulation and center-of-gravity offset analysis of the frame structure, and the results meet the design requirements.

## 2. Analysis of Spider Locomotion Behavior

For the purpose of adapting to a variety of natural environments, spiders have evolved a variety of movement characteristics, including crawling, running, jumping, rolling, swim-

ming and flying. These modes of movement allow spiders to move across a wide variety of terrain, even in challenging environments such as rugged mountains, dangerous cliffs, and complex jungles with agility and speed. Numerous researchers, dedicated to in-depth studies to develop robots capable of displaying similar movement abilities in extreme environments, draw inspiration from the unique movement features of spiders for innovative design in biomimetic robot technology. For example, Xin H [29,30] observed spider locomotion on different pavement test platforms, comprising horizontal hard pavement, horizontal soft pavement, and sloped soft pavement. They analyzed the joint kinematics and driving modes of spiders under different ground conditions. Wang Z. Y. [31] studied and analyzed the movement behavior of huwena bird-clawed spiders on the horizontal plane by using test channels, high-speed cameras and a computer-based three-dimensional motion observation system, and believed that the movement speed of bird-clawed spider was mainly achieved by increasing step frequency. Compared to other insects, spiders exhibit better movement stability. During movement, the speed and height of the center of mass exhibit periodic fluctuations, with maximum values occurring during the phase of alternating leg support and minimum values during the stable support phase. Jonas O. Wolff [32] conducted research on the kinematics and dynamics of arachnids and he proposed the integration of robotics with arachnid studies. Carlo M. Biancardi [33] simplified the model of individual spider legs by capturing and analyzing large spiders' biomechanics. Landkammer S. [34] studied the leg joints of spiders and found that the leg movement of spiders did not rely on the muscle system, but relied on the hydraulic system of the legs, using a variety of devices and methods to observe the behavior of spiders in real time and analyze their movement patterns. Although this research has made significant progress, the relationship between the physiological structure of spiders and their locomotion mechanisms remains unclear.

To better optimize the design of biomimetic spider robots, it is necessary to analyze the body structure and movement mechanisms of spiders in the natural world, providing a reference for the development of biomimetic spider robots. This paper delves into the analysis of the spider's movement mechanism, including its physiological structure, leg drive mechanism, and gait, thereby enhancing the adaptability and efficiency of biomimetic spider robots in complex environments.

### *2.1. Analysis of Spider Physiological Structure and Leg Drive Mechanism*

The structure of a spider's body and legs is shown in Figure 1a,b.The extension of the spider's legs primarily relies on its hydraulic mechanism (the spider's leg joints contain a unique muscle structure capable of storing and releasing hydraulic pressure). When a spider wishes to extend a leg, it uses this muscle to pressurize the fluid into the joint, thereby straightening the leg. Spiders flex their legs by contracting their leg muscles. During the leg contraction movement, the neural network transmits signals to control the contraction of the leg muscles and drive the vertical rotation of the femur. Due to the rotation, the patella, tibia, basal bone, femur end and paw are driven to achieve vertical contraction and complete the leg lift action. Thus, the rotation of the tibia, basal femur, and distal femur allows for the spider to achieve a leg-bending motion. At the same time, the rotation of the paw can adjust the degree of contact pressure with the ground.

In addition to vertical movement, spiders can also move their legs horizontally. The horizontal movement of spiders' legs mainly relies on the horizontal rotation of the base segment, pushing the femur, patella, tibia, base segment, distal femur and claw to move in the horizontal direction so that the legs can complete the forward and backward movement. This unique mode of movement ensures that the spider can adapt to a variety of complex environments, not only helping to capture prey, but also helping the spider to escape from predators.

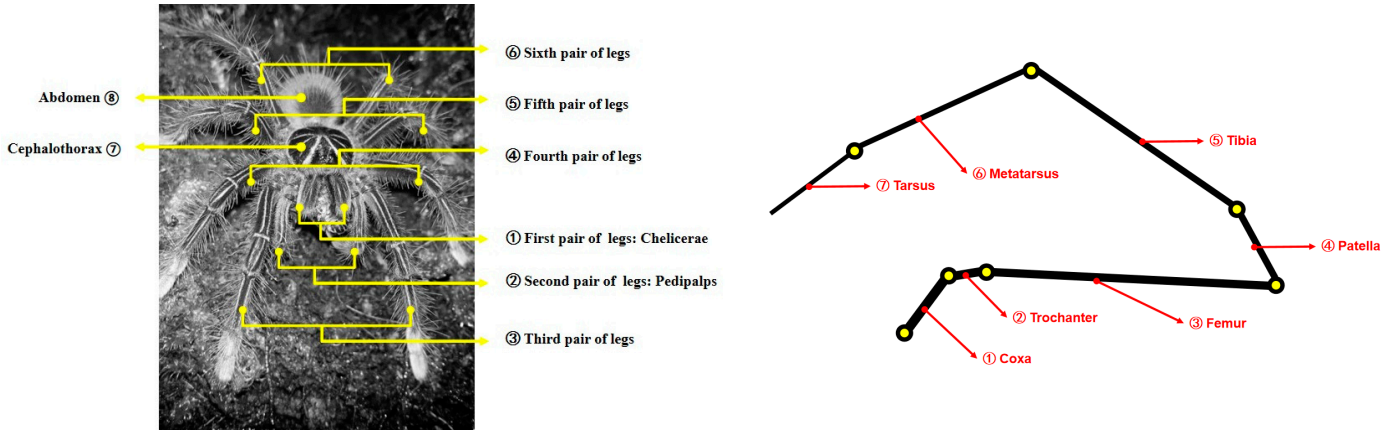



**Figure 1.** (**a**) The structure of a spider body; (**b**) the structure of a spider leg.

## *2.2. Gait Analysis*

### 2.2.1. Spider Locomotor Gait

A spider's gait is not a simple random movement, but a highly coordinated process, which ensures its stability and agility in the movement process. Spiders have eight legs, and the synergy of these legs allows them to walk flexibly on a variety of different surfaces. When they move, they usually lift four legs off the ground, while the other four remain in contact to support their bodies. The system allows them to move precisely and respond quickly to any threats or changes in the environment. In addition, spiders can change direction quickly and effectively by alternating leg movements, which are essential for catching prey and avoiding danger. In short, the sport pattern of a spider is a complex process of coordination and adaptation that demonstrates a remarkable fusion of stability, speed, and potential. Suter R. B. [35] found that spiders of different families and genera use different gaits during their movement. For example, Dolomedes triton of the Pisauridae family has a gait specifically designed for movement in water. Biancardi C. M. [33] noted that spiders use different movements when moving slowly or fast, with four-legged movements in slow movements, and actions in rapid movements are more complicated. In addition, spiders move rapidly, exhibiting different step patterns in the front pairs and the rear pairs of legs, and more irregular steps in the back pairs. Spagna J. C. [36] also observed that spiders used alternating movements of the four legs when running, distributing them in incorrect pairs along the body axis, forming alternating four-legged steps. Nevertheless, the latter two pairs of leg movement laws are different from the first two pairs; it is more difficult to judge their specific step information, so in the simulation mechanics, there is a greater degree of difficulty. Guo S et al. [37] elaborated on the quadruped gait in detail and used it to complete the relevant control analysis of its servo, but they simplified the complexity of the leg movement to make its movement posture similar, thereby completing the movement design.

### 2.2.2. Triangle Gait

The spider-like robot design process offers two options: a six-foot robot and an eight-foot robot. In comparison, the former is arranged in a uniform and surrounding manner, the load-bearing uniformity of each leg is better, the movement flexibility is better, and the control difficulty and cost are reduced. The latter has a more complex structure and more support points but is heavier. Therefore, we chose the six-legged bionic spider robot as the design object.

By imitating the triangular gait of insects, the six-legged robot can complete movements such as walking and crossing obstacles on complex terrain, while having high mobility and stability. This kind of robot with triangular gait has good symmetry and simplicity, which can reduce the complexity of control requirements and improve operation

efficiency. Grabowska M. [38] and Bender J. A. [39] divide the six legs into two groups to form two triangular brackets. When all the legs of one triangular bracket are lifted at the same time, the three legs of the other triangular bracket remain stationary to support the body. In this process, muscle contraction drives the body forward and causes the body to rotate slightly with the fulcrum as the center of rotation. Then, the other triangular bracket repeats the previous action, and the two groups of brackets rotate with each other to achieve forward movement. Its walking trajectory is a zigzag curve. The specific process of walking is shown in Figure 2. In Figure 2a, 2-4-6 legs are lifted and moved forward, completing the specified movement as indicated in Figure 2b, with the 1-3-5 legs lifted up and moved forward, completing the movement as shown in Figure 2c.

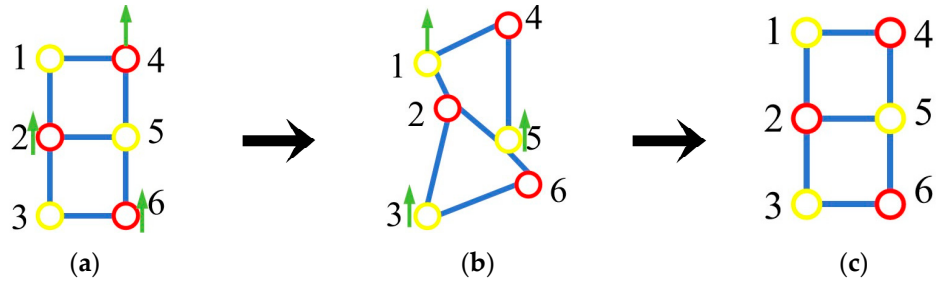



**Figure 2.** Schematic diagram of triangular gait operation, (**a**) initial state diagram; (**b**) motion process state diagram; (**c**) final state diagram.

Placing the center of gravity within the triangle ensures the stability of a support triangle with three different legs. However, the shape of the triangle, like isosceles triangles with a vertex angle of 65° or 60°, or irregular triangles, also influences the stability of the biomimetic robot. Three equilateral triangular features that can achieve center coincidence represent the highest level of stability. As long as the robot maintains this triangular state while walking, its overall stability will be optimal. However, due to the irregular terrain characteristics of disaster areas, jungles, cliffs and other actual terrain, the robot is difficult to control when landing, and cannot form the above equilateral triangle state. In this paper, MATLAB software is used to simulate the center of gravity of the triangle, and the change in center of gravity with the structure parameters is analyzed, finding that the change occurred due to the different position of the foot. We use this information to communicate with the control program to adjust the stability of its overall center of gravity, ensuring that the bionic spider robot has enough stability during the process of moving forward, and can adjust various gestures for different situations. The following chapters will deeply analyze the leg structure and body structure of the legs and body of the bionic spider robot.

## 3. Design and Analysis of Structure

In this chapter, the leg structure is designed with two degrees of freedom as the goal, and the body frame structure is selected considering the change in the body's center of gravity. The specific analysis and design process is as follows.

### *3.1. Design and Analysis of Leg Structure*

#### 3.1.1. Degree of Freedom Analysis

In the design of biomimetic spider robots, the number of DOFs in the leg mechanism is crucial for their ability to travel smoothly over rough terrain and walk rapidly on flat surfaces. Mechanically, the execution of complex movements increases with the number of DOFs. For biomimetic spider robots, the ability to perfectly replicate spider walking actions allows for adapting to most environments. However, in terms of control, the increase in DOFs necessitates independent control for each leg to meet the needs of different environments, which in turn complicates the robot's control system. It is necessary to consider the coupling relationship between the control systems of the legs and deploy appropriate sensors to assist in identifying the robot's state. Both the cost and the complexity of the

data will increase. If we combine the analysis from Section 2 with both aspects, the spider's leg movements can be simplified into two movements: swinging and lifting. The two-DOF structure is simple and effectively improves the above problems. Kyberd P.J. et al. [40] developed a two-DOF hand prosthesis with layered control and microprocessor-based fine tuning that simplifies the operator's control requirements and has some usability. Umeno et al. [41] introduced a speed control system for DC servomotors that utilizes a two-DOF controller parametrization to enhance closed-loop system performance, including disturbance suppression and robustness to parameter variations, while maintaining the command input response. Maalouf D. et al. [42] propose a classification framework for two-DOF mechanical systems that prioritizes the largest feedback linearizable subsystem with internal stability and highlights the significance of generalized conjugate momenta in achieving stable closed-loop systems. These studies have pointed out the advantages of two DOFs.

According to the analysis of the triangular gait in Section 2.2.2, we call the group that provides support the support phase and the other group the swinging phase.

The legs are divided into two structural units with 1 degree of freedom. In this configuration, structural unit I performs a lifting action on the vertical plane and structural unit II performs a swinging action on the horizontal plane. The simplified process of the legs in this study is shown in Figure 3.

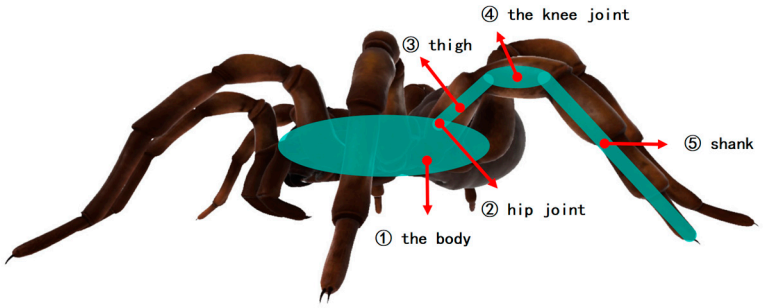



**Figure 3.** Spider leg joint motion diagram.

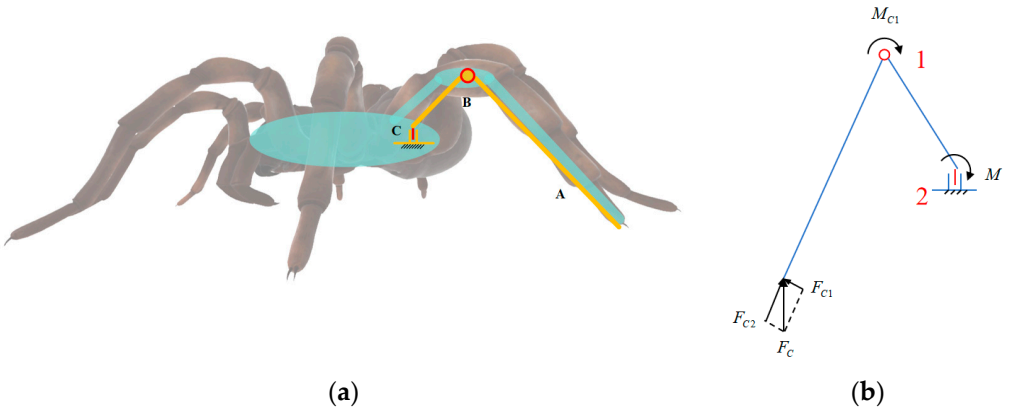
In Figure 3, the body, thigh, and shank are, respectively, labeled as ①③⑤, while the knee joint and hip joint are labeled as ②④. The two-DOF mechanism is equivalent to its actuation components; therefore, actuators are placed at the hip joint and knee joint. Nonetheless, the knee joint will be subjected to forces from other directions, which can affect the motor's working load and stable torque output. In the following section, we will discuss the new mechanism developed in this study to address this issue.

#### 3.1.2. Structural Analysis

Figure 4a is a simplified schematic of the leg mechanism derived from the analysis of Figure 3; the red sections B and C represent the knee and hip joints. We perform a force analysis on the schematic diagram of the leg mechanism based on the contents of Section 3 in *Machine Design* by Robert L. Norton [43]. In Figure 4b, the motor at location 1 is subjected to not only torque $M_{C1}$ but also a radial force $F_{C2}$, which is a component of the force $F_C$, exerted on the motor. At location 2, the force $F_C$ generates a bending moment $M$ on the motor's output shaft.

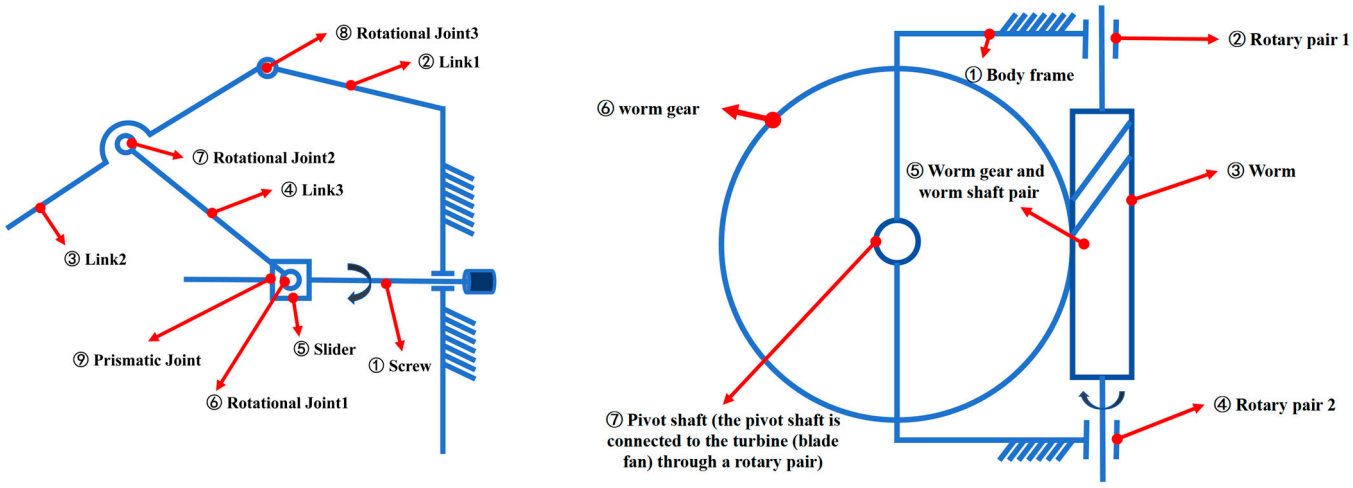
It is necessary to optimize the design of this structure in light of the robot's own weight, the various devices it must carry under various operating scenarios, and the types of motors it can choose from. We carry out the following structural optimization designs for structural units I and II.

Structural unit I: As shown in Figure 5a, adjust the position of the power source and adapt the structure of rods AB and BC in Figure 4a to form a new leg-lifting mechanism.




(**a**) (**b**)

**Figure 4.** (**a**) Schematic diagram of the overall leg structure; (**b**) force analysis of the leg.




(**a**) (**b**)

**Figure 5.** (**a**) Schematic diagram of structural unit I; (**b**) schematic diagram of structural unit II.

As depicted in Figure 5a, the motor drives the screw as the driving element. Since the slider is restricted, it will not rotate by itself. When the leg is under force, the motor does not need to be in a stalled state, which reduces the loss of the motor. In addition, the support structure should be used as a direct load-bearing unit for the screw, and the motor has no additional load loss. When designing the screw, we adopted a large pitch to ensure that it withstands a large load and degrades the motor selection requirements.

Freedom degree analysis is conducted for this mechanism. We adopted the planar freedom degree calculation formula, i.e., Equation (1), to analyze the freedom degree of structural unit I, given that components 2 and other mechanisms are in parallel planes:

$$F = 3n - 2P_l - P_h \tag{1}$$

In Equation (1), $F$ is the degree of freedom, $n$ is the number of active components, $p_l$ is the number of lower-pair joints, and $p_h$ is the number of higher-pair joints.

Consequently, the degree of freedom $F_1$ at structural unit I is 1.

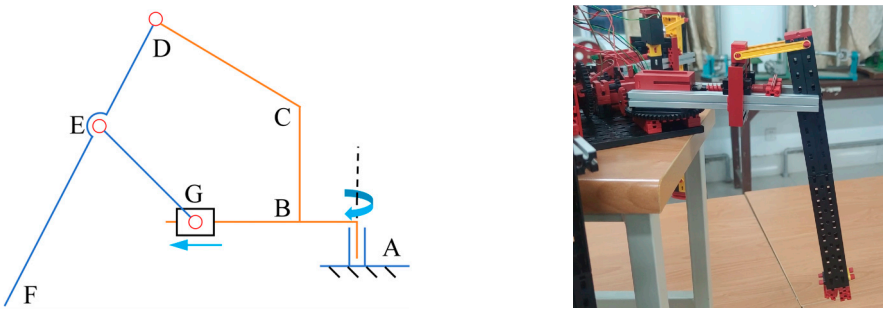
As displayed in Figure 5b, the motor drives the worm as the driving element. The self-locking performance of the worm gear mechanism can ensure that the leg will not rotate when it is stationary, and the motor does not need to be in a stalled state; then, since the maximum rotation angle is 120 degrees, the larger transmission ratio can reduce the starting torque of the motor and provide a sufficient torque, so as to achieve a fast and powerful rotation of the leg and reduce the selection requirements of the motor.

Similarly, the degree of freedom $F_2$ of structural unit II is 1.

In summary, the degree of freedom of each mechanical leg is $F = F_1 + F_2 = 2$, which meets the freedom design requirements of Section 3.1.1 for the movement of the leg.

3.1.3. Kinematic Analysis

Based on the analysis in Section 3.1.2, a simplified motion diagram of the leg mechanism is provided in Figure 6. We conduct the kinematic analysis of the selected mechanism to determine whether the touchdown points and their motion rates in the leg comply with the design requirements. We then optimize the mechanism to address any potential issues that may arise.




(**a**) (**b**)

**Figure 6.** (**a**) Schematic diagram of the leg mechanism motion; (**b**) physical prototype of the leg structure.

In Figure 6, point A represents the rotational center for the leg's swinging motion, where the slider performs a reciprocating motion. Point G is the center of the slider and the connection point with the connecting rod. When performing kinematic analysis of the mechanical structure, since rod BCD has a minimal impact on kinematics due to its shape, which serves only for structural reinforcement and has fixed parameters, it can be simplified to rod BD. This simplification makes the diagram clearer, as illustrated in Figure 7.

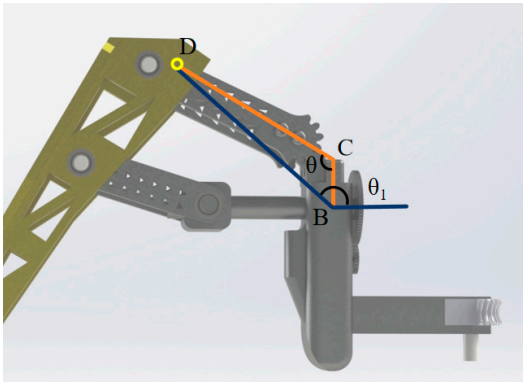



**Figure 7.** Analysis simplification.

For convenient subsequent calculations, the definitions of the parameters for Figures 6 and 7 are summarized in Table 1 below.

The definitions of rod length BD, $l_7$, and angle ABD, $\theta_1$, are given in Formula (2) and Formula (3), respectively.

$$l_7 = \sqrt{{l_3}^2 + {l_2}^2 - 2 \times l_2 \times l_3 \times \cos \angle\theta} \quad (2)$$

$$\theta_1 = \arcsin(l_3 \times \sin(\angle\theta)/l_7) + \pi/2 \quad (3)$$

**Table 1.** Intrinsic parameters of the leg mechanism.

| Serial Number | Name | Symbol |
|---|---|---|
| 1 | AB | $l_1$ |
| 2 | BC | $l_2$ |
| 3 | CD | $l_3$ |
| 4 | DE | $l_4$ |
| 5 | EG | $l_5$ |
| 6 | EF | $l_6$ |
| 8 | ∠BCD | $\theta$ |

Hence, the coordinate frames for each leg of the biomimetic spider robot are established, respectively, as $\sum O_A$, where A represents the legs. Additionally, the body coordinate frame, $\sum O_R$, is established, where R represents the body, as shown in Figure 8. Based on this, the kinematic analysis of the biomimetic spider robot is carried out step by step.

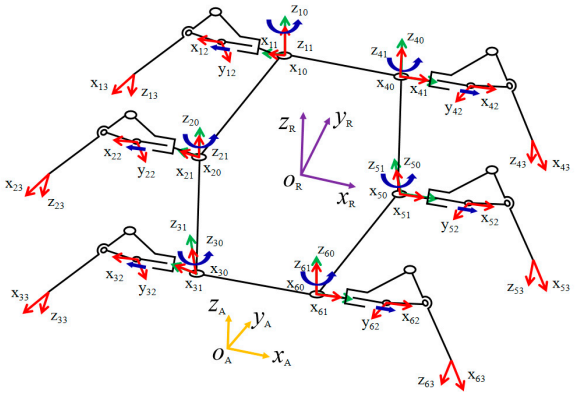


**Figure 8.** Simplified coordinate system model.

The improved Denavit–Hartenberg (D-H) parameters are used to analyze the changes in the foot end coordinates of the legs and their dynamic characteristics. The robot leg motion is shown in Figure 9.

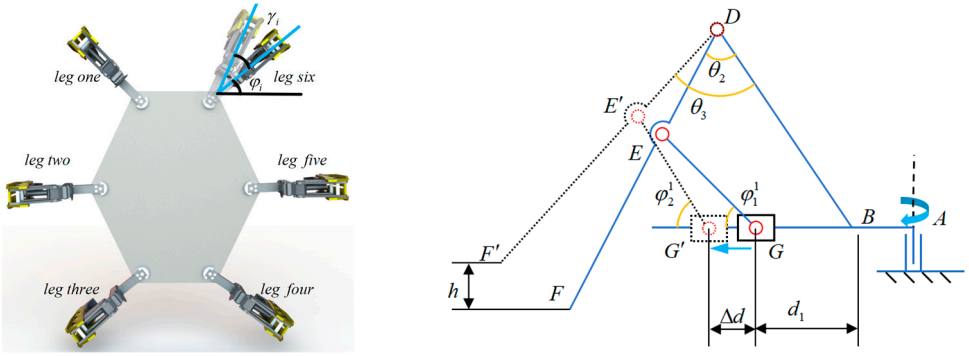



**Figure 9.** (**a**) The swing angle of the *i*-th leg; (**b**) the lift height of the *i*-th leg.

The initial parameters involved in Figure 9 are shown in Table 2. The drive mechanism parameters are analyzed, thereby determining the D-H-related parameters of the leg mechanism.

**Table 2.** Initial parameters of the leg.

| Symbol | Description |
|---|---|
| $\phi_i$ | Initial installation angle of the *i*-th leg. |
| $\phi_1^1$ | Initial angle between link EG and the slider. |
| $\theta_2$ | Initial installation angle between rocker DF and rod BD. |
| $d_1$ | Initial distance between the slider and point B. |
| $i_1$ | Transmission ratio of the worm gear. |
| $P$ | Screw pitch. |

The swing angle $\gamma_1$ of the leg is defined as shown in Equation (4).

$$\gamma_1 = 2\pi \times \frac{n_1}{i_1} \times t \tag{4}$$

where $n_1$ represents the rotational speed of the oscillating drive motor. Since the motor is connected to the worm, $n_1$ is equal to $n_{\text{worm}}$. $t_1$ is the operating time of the motor, and the distance $\Delta d$ for the slider's movement is defined as shown in Equation (5).

$$\Delta d = n_2 \times p \times t_2 \tag{5}$$

In the above formula, $n_2$ denotes the rotational speed of the leg drive motor, and $t_2$ represents the operating time of the motor.

According to geometric theory, a new parameter is introduced; $l'$ represents the length of DG, and the changes in $\phi_2^1$ and $\theta_3$ during the leg movement are analyzed as follows:

$$l' = \sqrt{{l_7}^2 + (d_1 + \Delta d)^2 + 2l_7(d_1 + \Delta d)\cos\theta_1} \tag{6}$$

$$\phi_2^1 = \pi - (\arccos\frac{{l'}^2 + (d_1 + \Delta d)^2 - l_7^2}{2l'(d_1 + \Delta d)} + \arccos\frac{{l'}^2 + {l_5}^2 - l_4^2}{2l'l_5}) \tag{7}$$

$$\theta_3 = \arccos\frac{{l'}^2 + l_7^2 - (d_1 + \Delta d)^2}{2l'l_7} + \arccos\frac{{l'}^2 + {l_4}^2 - l_5^2}{2l'l_4}) \tag{8}$$

From Table 3, it is known that the coordinate transformation matrix between bar AB and the base is defined as shown in Equation (9).

$${}_0^1T_A = \begin{bmatrix} \cos(\gamma_1) & -\sin(\gamma_1) & 0 & l_1 + d_1 \\ \sin(\gamma_1) & \cos(\gamma_1) & 0 & 0 \\ 0 & 0 & 1 & 0 \\ 0 & 0 & 0 & 1 \end{bmatrix} \tag{9}$$

**Table 3.** Denavit–Hartenberg (D-H) parameter table.

| Serial Number | $a$ | $\alpha$(○) | $d$ | $\beta$(○) | Description |
|---|---|---|---|---|---|
| 0 | 0 | 0 | 0 | 0 | The base corresponds to the joint between the leg and the body pin axis. |
| 1 | $l_1 + d_1$ | 0 | 0 | $\gamma_1$ | Link AB exhibits oscillatory motion. |
| 2 | 0 | 90 | $\Delta d$ | 0 | The slider undergoes translational motion. |

The transformation matrix between the slider and the left link is defined as shown in Equation (10).

$${}_1^2T_A = \begin{bmatrix} 1 & 0 & 0 & \Delta d \\ 0 & 1 & 0 & 0 \\ 0 & 0 & 1 & 0 \\ 0 & 0 & 0 & 1 \end{bmatrix} \tag{10}$$

From the above, Equation (11) can be derived.

$$ {}^{2}_{0}T_{A} = \begin{bmatrix} \cos(\gamma_1) & -\sin(\gamma_1) & 0 & l_1 + d_1 \\ \sin(\gamma_1) & \cos(\gamma_1) & 0 & 0 \\ 0 & 0 & 1 & \Delta d \\ 0 & 0 & 0 & 1 + l_1 + d_1 \end{bmatrix} \tag{11} $$

In Equation (11), the term $1 + l_1 + d_1$ represents the displacement of slider G from its initial position on the link to a distance $\Delta d$. The initial position of the slider on the link is at a distance of $l_1 + d_1$ from the rotational center of the link. Therefore, the final position of the slider after movement is the sum of the initial distance and the distance it moves along the link. Since the coordinates of the foot can be represented in a coordinate system with the slider as the origin, they can be subsequently transformed into the desired coordinate system.

In the slider coordinate system, the coordinates of foot F are $(x_3, y_3, z_3)$, which are defined, respectively, in Equation (12).

$$ \begin{cases} x_3 = (l_4 + l_6) \cdot \cos(\theta_1 - \theta_3) - l_7 \cdot \cos\theta_1 - (d_1 + \Delta d) \\ y_3 = 0 \\ z_3 = l_7 \cdot \sin\theta_1 - (l_4 + l_6) \cdot \sin(\theta_1 - \theta_3) \end{cases} \tag{12} $$

The $i$-th leg coordinate system $\sum O^i_A$ is represented in the body coordinate system $\sum O_B$ as Equation (13).

$$ {}^{A}_{B}T^{i} = \begin{bmatrix} \cos\phi_i & -\sin\phi_i & 0 & p^i_{Ax} \\ \sin\phi_i & \cos\phi_i & 0 & p^i_{Ay} \\ 0 & 0 & 1 & p^i_{Az} \\ 0 & 0 & 0 & 1 \end{bmatrix} \tag{13} $$

In Equation (13), $\phi_1$ represents the angle between the x-axis of leg coordinate frame $\sum O^i_A$ and the x-axis of the body coordinate frame $\sum O_B$, which is the initial installation angle. The coordinates $(p^i_{Ax}, p^i_{Ay}, p^i_{Az})$ denote the position of the base of $i$-th leg, which is the origin of the leg coordinate frame, in the body coordinate frame. Furthermore, the transformation matrix between the leg coordinate frame and the body coordinate frame is analyzed, as shown in Equations (14) and (15).

$$ {}^{2}_{0}T^{i}{}_{B} = {}^{A}_{B}T^{i} \cdot {}^{2}_{0}T_{A} \tag{14} $$

$$ {}^{2}_{0}T^{i}{}_{B} = \begin{bmatrix} \cos(\phi_i + \gamma_1) & -\sin(\phi_i + \gamma_1) & 0 & \cos\phi_i \cdot (l_1 + d_1) + p^i_{Ax} \\ \sin(\phi_i + \gamma_1) & \cos(\phi_i + \gamma_1) & 0 & \sin\phi_i \cdot (l_1 + d_1) + p^i_{Ay} \\ 0 & 0 & 1 & p^i_{Az} \\ 0 & 0 & 0 & 1 \end{bmatrix} \tag{15} $$

Consequently, through forward kinematics, the position of the foot tip in the body can be determined. The foot tip coordinates $(x_3, y_3, z_3)$ are transformed into $(x_B, y_B, z_B)$, as shown in Equation (16).

$$ \begin{cases} x_B = x_3 \cdot \cos(\phi_i + \gamma_1) - y_3 \cdot \sin(\phi_i + \gamma_1) + P^i_{Ax} \\ y_B = x_3 \cdot \sin(\phi_i + \gamma_1) + y_3 \cdot \cos(\phi_i + \gamma_1) + P^i_{Ay} \\ z_B = z_3 + P^i_{Az} \end{cases} \tag{16} $$

In Equation (16), $(x_B, y_B, z_B)$ represents the coordinates of the foot tip in the body coordinate frame $\sum O_B$.

#### 3.1.4. Inverse Kinematics

Using Equation (16), the coordinates of the foot tip $(x_B, y_B, z_B)$ are obtained. Based on the relationships between the various links, the rotational angles of the two drive motors

during operation are analyzed. By rearranging and expanding Equation (16), we derive Equation (17).

$$\begin{cases} \frac{x_B - P^i_{Ax}}{(l_4+l_6)\cdot\cos(\theta_1-\theta_3)-l_7\cdot\cos\theta_1+(d_1+l_1)+\Delta d} = \cos(\phi_i+\gamma_1) \\ \frac{y_B - P^i_{Ay}}{(l_4+l_6)\cdot\cos(\theta_1-\theta_3)-l_7\cdot\cos\theta_1+(d_1+l_1)+\Delta d} = \sin(\phi_i+\gamma_1) \\ \frac{z_B - l_7\sin\theta_1 - P^i_{Az}}{l_4+l_6} = \sin(\theta_1-\theta_3) \end{cases} \quad (17)$$

For Equation (17), algebraic substitutions are performed, letting

$$a = l_7\cdot\cos\theta_1 - d_1 - l_1, b = l_4 + l_6, c = x_B - P^i_{Ax}, d = y_B - P^i_{Ay}, e = z_B - P^i_{Az} - l_7\sin\theta_1, e = z_B - P^i_{Az} - l_7\sin\theta_1 \quad (18)$$

Then, we substitute Equation (18) into Equation (17) and obtain Equation (19).

$$\Delta d = a - \sqrt{b^2 - e^2} + \sqrt{c^2 + d^2} \quad (19)$$

The rotation of the leg lift motor is transmitted through a nut and screw mechanism, resulting in the movement distance of the slide block. Consequently, the operational rotation angle $\varphi_2$ of the leg lift motor can be determined as shown in Equation (20).

$$\varphi_2 = 2\pi\cdot\Delta d/P \quad (20)$$

Substituting Equation (19) into Equation (17) yields Equation (21).

$$\frac{d}{\sqrt{c^2+d^2}} = \sin(\phi_i+\gamma_1) \quad (21)$$

Due to the transmission of the swing motor through a worm gear and worm shaft mechanism, the motor rotation angle $\varphi_1$ can be analyzed from the transmission ratio, as shown in Equation (22).

$$\varphi_1 = i_1\cdot(\arcsin\frac{d}{\sqrt{c^2+d^2}} - \phi_i) \quad (22)$$

Through the kinematic analysis of the legs, it can be seen that the movement trajectory of the legs is determined not only by the operating parameters of the motor, but also by the design parameters of different components. The detailed analysis is shown in Section 4.

### *3.2. Design and Analysis of Body Structure*

#### 3.2.1. Overview

As is known from Section 3.1, the connection point between the leg mechanism and the body is the hip joint position in the physiological structure of spiders. As illustrated in Figure 10, there are two spiders with different habits: a is a spider of the family Theridiidae, which excels at hunting with webs; b is a wolf spider, which hunts on the ground.



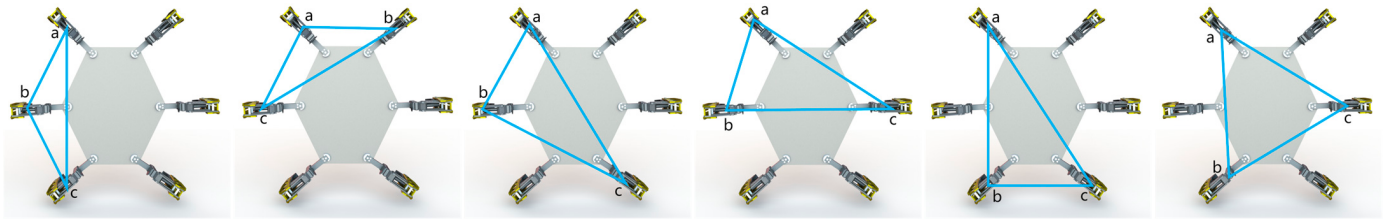
(**a**) (**b**)

**Figure 10.** The connection between the body and legs in spiders with various habits: (**a**) linyphiidae spider; (**b**) wolf spider.

It is observable that the spacing between the hip joints of the former is smaller than that of the latter, which is convenient for the former to reduce its own mass and provide a stable posture on the spider web. The latter usually moves on the ground and requires higher explosive power when hunting and moving. At this time, its leg length is shorter than the former, and the farther hip joint position facilitates its rapid movement. The layout positions of both are similar to ellipses. In the design process of the hexapod bionic robot body, the hip joint position is used as the outer edge contour of the robot body. There are three ways in conventional design which will be analyzed in this section to obtain the optimal outer edge contour as the body structure.

### 3.2.2. Analysis of Support Triangle Gait

According to the findings of Section 2.2.2 in this paper, the biomimetic spider robot employs a triangular gait for walking. In existing research, many scholars have also adopted the triangular gait as the walking gait for biomimetic robots, such as Guo, Y.Q. [44], Zhang, Y. [45], Ni, Y. [46], etc., who have all used the triangular gait in the walking control of their designed hexapod robots. However, the triangular configurations chosen and the different legs that form the triangle vary during the design process. If only the different legs that form the triangle are considered, there are six possible configurations, as shown in Figure 11, the point a,b,c represent the three vertices of a triangle.




(**a**) (**b**) (**c**) (**d**) (**e**) (**f**)

**Figure 11.** Six types of support triangles, (**a**) the triangle formed by legs on one side, (**b**) the triangle formed by two front legs and a middle leg, (**c**) the triangle formed by the front and middle leg on one side and the rear leg on the other side, (**d**) the triangle formed by two middle legs and a front leg, (**e**) the triangle formed by two rear legs and a front leg, (**f**) the triangle formed by the front and rear leg on one side and the middle leg on the other side.

The triangle structure in Figure 11 is expressed in a matrix to assist in judging its stability margin. An equilateral hexagon is selected as the prototype of the support triangle analysis. Its side length is $2m$, and it corresponds to Figure 11a–f, respectively.

$$\begin{pmatrix} -m & \sqrt{3}m \\ -2m & 0 \\ -m & -\sqrt{3}m \end{pmatrix} \quad \begin{pmatrix} -m & \sqrt{3}m \\ m & \sqrt{3}m \\ 2m & 0 \end{pmatrix} \quad \begin{pmatrix} -m & \sqrt{3}m \\ -2m & 0 \\ m & -\sqrt{3}m \end{pmatrix} \quad \begin{pmatrix} -m & \sqrt{3}m \\ -2m & 0 \\ 2m & 0 \end{pmatrix} \quad \begin{pmatrix} -m & \sqrt{3}m \\ -m & \sqrt{3}m \\ 2m & 0 \end{pmatrix} \quad \begin{pmatrix} -m & \sqrt{3}m \\ -m & -\sqrt{3}m \\ 2m & 0 \end{pmatrix}$$

(**a**) (**b**) (**c**) (**d**) (**e**) (**f**)

In the triangles shown in Figure 11a,b, the center of gravity (COG) of the support triangle is located outside the triangle, and the stability margin is negative, indicating that the robot cannot maintain stability in the posture, hence this method is unreasonable. In the cases shown in Figure 11c–e, the support triangle passes through the center of gravity, and the stability margin is in a critical state. In this situation, the probability of the robot tipping over is high, which is not conducive to the robot's movement on uneven roads and reduces the robot's traversability. However, stability can be improved through stability-enhancement measures; thus, these support triangles are reasonable. In the support triangle shown in Figure 11f, the center of gravity of the legs on one side and the middle leg on the other side is located inside the triangle, and its stability margin is the best among the five support triangles mentioned earlier, indicating the best stability. This represents the maximum expectation for support, making this scheme the most reasonable. Liu Y [47] conducted a study on the influence of center-of-gravity alterations on the walking stability

of hexapod biomimetic mechanical devices and focused on center-of-gravity trajectory planning. The research also addresses control methods to ensure overall stable walking when any one of the six legs is problematic.

#### 3.2.3. Analysis of the Layout of Body and Leg Connection Points

After performing kinematic forward and inverse analyses of the legs, considering the impact of the installation position of the legs on the overall machine's motion performance and load-bearing capabilities, an analysis of the connection points between the legs and the body is conducted, with a primary focus on the position of the center of gravity, etc. In calculating the position of the center of gravity, the relationship between the triangle's coordinate positions and the center of gravity is utilized, as shown in Equation (23).

$$\overline{x} = \frac{\int x d\sigma}{\int d\sigma}; \overline{y} = \frac{\int y d\sigma}{\int d\sigma} \tag{23}$$

In the case where the coordinates of the triangle are known, the central position of the triangle can be determined using Formula (24).

$$x_z = \frac{x_1 + x_2 + x_3}{3}; y_z = \frac{y_1 + y_2 + y_3}{3} \tag{24}$$

In Equation (24), $(x_z, y_z)$ represents the coordinates of the center of gravity, while $(x_1, y_1)$, $(x_2, y_2)$, and $(x_3, y_3)$ correspond to the vertices of the triangle. This approach is numerically straightforward in principle, yet its complexity arises in the acquisition of the coordinate information at the foot's endpoint. Due to the unknown environmental information of the biomimetic spider robot and the inability to predict the conditions of the landing site during rapid movement, whether it is on yielding ground or slippery surfaces, controlling the placement of the foot's endpoint is quite challenging.

In conclusion, this paper intends to reduce the size of the support triangle by defining its position at the connection points between the leg mechanism and the body, namely $a_1 \sim a_3$, $b_1 \sim b_3$, to determine its location, as shown in Figure 12. This arrangement forms a triangle between the support phase and the body's connecting part, which stabilizes the center of gravity of the body within the triangle. Consequently, this ensures that the overall center of gravity of the biomimetic spider robot remains within the support triangle formed by the foot end of the support phase.

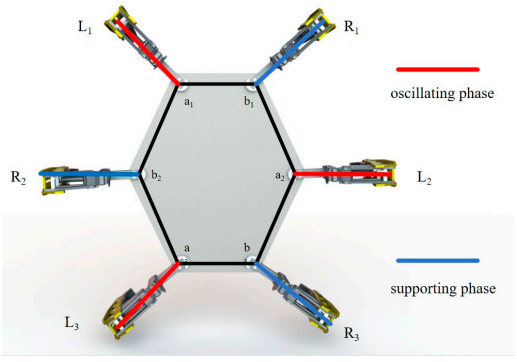



**Figure 12.** Support phase and swing phase.

In Figure 12, $L_1 \sim L_3$ represent the three legs in the swing phase, while $R_1 \sim R_3$ represent the three legs in the support phase. $a_1 \sim a_3$ and $b_1 \sim b_3$ are the connection points between the leg structures and the torso.

The common arrangements of the body–leg connections are shown in Figure 13. Figure 13a depicts legs on the same side not aligned on a straight line, with the middle leg on the outer side; Figure 14b shows legs on the same side aligned on a straight line; and

Figure 13c shows legs on the same side not aligned on a straight line, with the middle leg on the inner side.

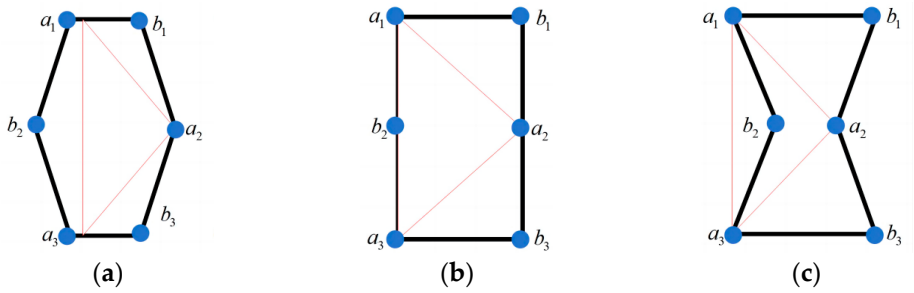



**Figure 13.** Body triangle, (**a**) convex hexagon; (**b**) rectangle; (**c**) concave hexagon.

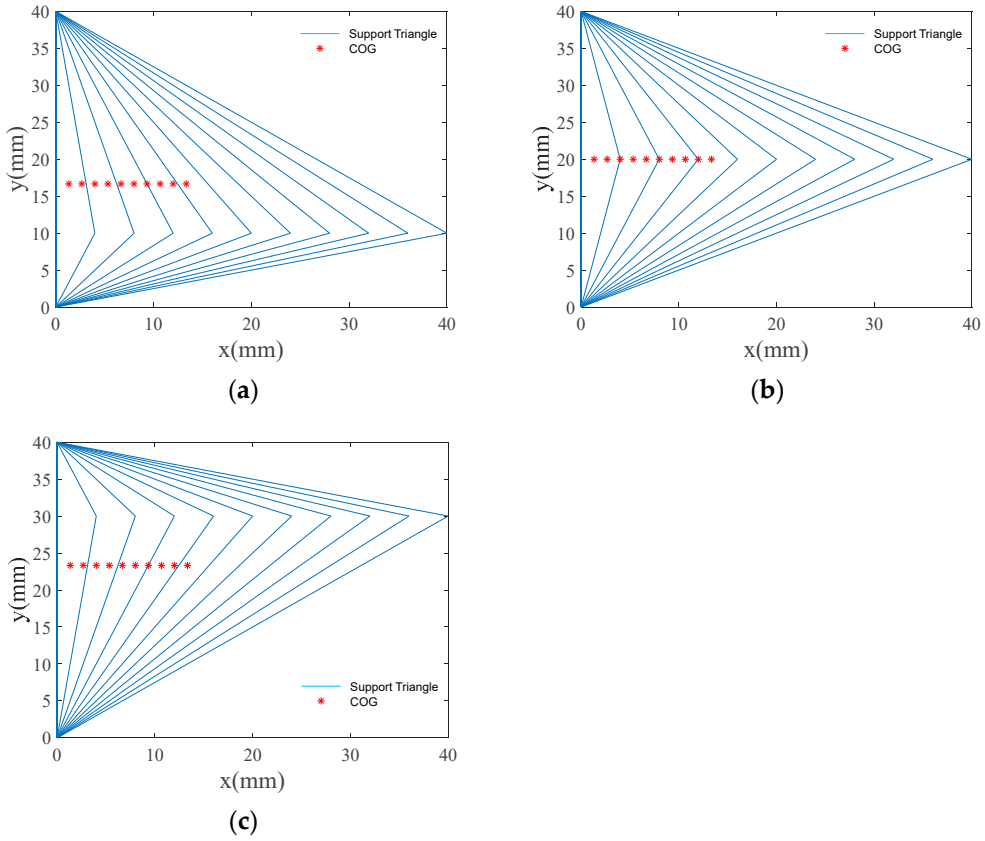



**Figure 14.** Center-of-gravity variation with y-axis coordinate: (**a**) y = 10; (**b**) y = 20; (**c**) y = 30.

When arranging the supporting triangle, if the overall width is the same, the distance from the vertex $a_2$ to the bottom $a_1a_3$ of the triangle in Figure 13b is the largest. In Figure 13a, $a_1a_3$ is located inside the frame, while in Figure 13c, it is located at the edge of the frame. It can be concluded that the center of gravity of the triangle is biased towards the bottom edge; compared to the c scheme, the center-of-gravity coincidence of the supporting triangles on both sides of the a scheme is higher.

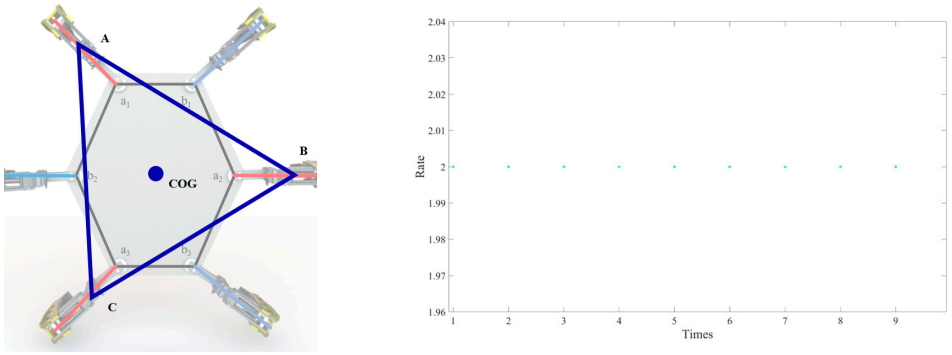
## 4. Simulation Experiment Analysis

### *4.1. Analysis of Body*

#### 4.1.1. MATLAB Simulation Analysis

Based on the analysis above, triangles with the same base length (all set to 40) were selected, where the x-axis coordinates of the vertices varied from 4 to 40, and the y-axis coordinates were 10, 20, and 30, respectively. A center-of-gravity traversal simulation of the biomimetic spider robot's body triangle was conducted in MATLAB, as shown in Figure 14.

From Figure 14, it is observed that when the x-axis coordinate remains constant, the center of gravity of the biomimetic spider robot's body triangle undergoes small amplitude variations, which are related to the y-axis coordinates of its vertices. This suggests that during the design process of the robot, if it is found that the center of gravity is too far forward or backward, the distance between the middle leg and the front and rear legs can be adjusted appropriately to ensure the stability of the robot's center of gravity. When the y-axis coordinate remains constant, the center of gravity moves further away from edge AB as the x-axis coordinate increases. At this point, due to the absolute position change in the center of gravity, the stability of the robot is also improved. However, as Figure 15a shows, the size of the triangle increases, making the robot's body larger, which is not conducive to its movement through dense forests and other environments.




(**a**) (**b**)

**Figure 15.** (**a**) Schematic diagram of triangle; (**b**) ratio of distance from center of gravity to point C to distance from COG to edge AB.

Figure 15a derived from Equation (25).

$$m = (x_3 - x_z)/x_z \tag{25}$$

In Equation (25), $m$ represents the ratio of the x-coordinate of the center of gravity to point B in Figure 15a and the edge AC, $x_3$ represents the x-coordinate value of point B, and $x_z$ represents the x-coordinate value of the center of gravity.

From Figure 15b, it can be concluded that the position of the center of gravity does not change relatively. The ratio of the distance from the center of gravity to a vertex to the distance from the center of gravity to the opposite side is two, which means the center of gravity always remains at one-third the height of the triangle. Therefore, regardless of the asymmetric arrangement of equipment on the body, the robot's center of gravity always leans towards one side. Based on this, simulation analyses were performed on the three schemes shown in Figure 13. As depicted in Figure 16, it is evident that in the scheme in Figure 13c, the center of gravity of the two sets of supporting triangles can never coincide. If the position of one set of center of gravity is determined, then during the locomotion of the biomimetic spider robot, the leg located in the middle, which is closer to the center of gravity, will bear a greater force than the other two legs, increasing the likelihood of a malfunction in that leg. Once this leg encounters a problem, the robot will be in a paralyzed state, which is detrimental to the execution of various tasks.

As shown in Figure 16, the convex hexagon makes it easier to consider aligning the center of gravity of the two groups of triangles, so that during the movement of the robot, no matter which group is in the support stage, the three legs can obtain equal support. This further ensures the stability of the robot, facilitates rapid movement, and reduces the overall wear of the robot.

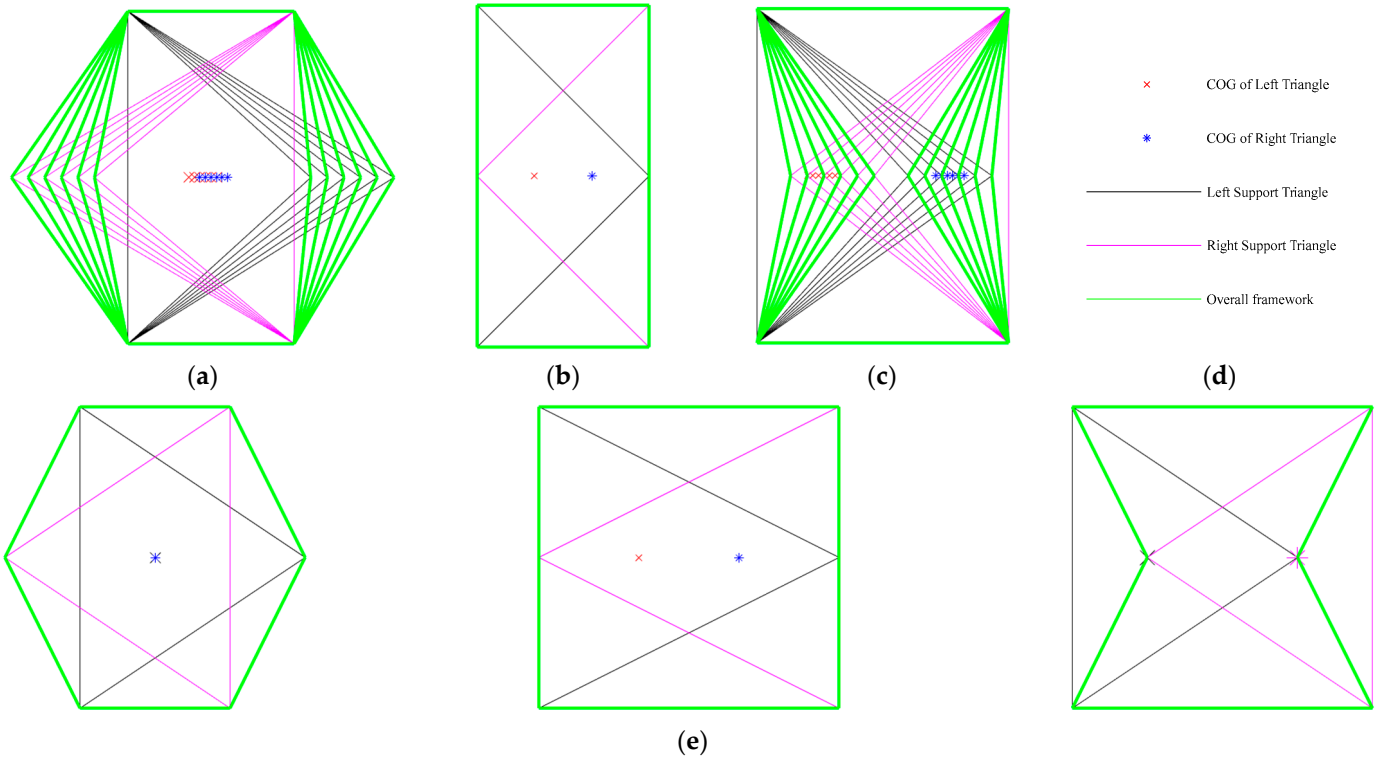



**Figure 16.** Scheme analysis, (**a**) convex hexagon; (**b**) rectangle; (**c**) concave hexagon; (**d**) legend; (**e**) comparative analysis of the scheme shown in Figure 13.

#### 4.1.2. Analysis and Comparison

Based on the above analysis, we have selected the body structure of the spider robot in Figure 16a, as shown in Table 4.

**Table 4.** Robotic architecture parameters.

| Symbol | Paraphrase | Parameter Values (mm) |
|---|---|---|
| S1 | Distance between points $a_1$ and $a_2$ | 120 |
| S2 | Distance between points $b_1$ and $b_2$ | 120 |
| S3 | Distance between line $a_1a_2$ and line $c_1c_2$ | 80 |
| S4 | Distance between line $b_1b_2$and line $c_1c_2$ | 80 |
| S5 | Distance between points $c_1$ and $c_2$ | 240 |
| S6 | Distance from point $c_2$ to line $a_1b_1$ | 60 |

The results of gravitational analysis and MATLAB analysis are shown in Figure 17.

As indicated in Figure 17, when the supporting triangles on both sides work alternately, the relative coordinates of the center of gravity do not change, so this scheme is stable during the robot movement. As the overall arrangement of the bionic spider robot presents a symmetrical feature, according to the analysis in Figure 14, it can be seen that the relative position of the center of gravity will change when the arrangement position of the middle leg is changed, that is, the distance from point c to $a_1a_2$ or $b_1b_2$. In the third process, the center of gravity will still coincide because its position changes in the y direction but does not change in the x direction. Thus, it is convenient to arrange the controller and power supply on the body.

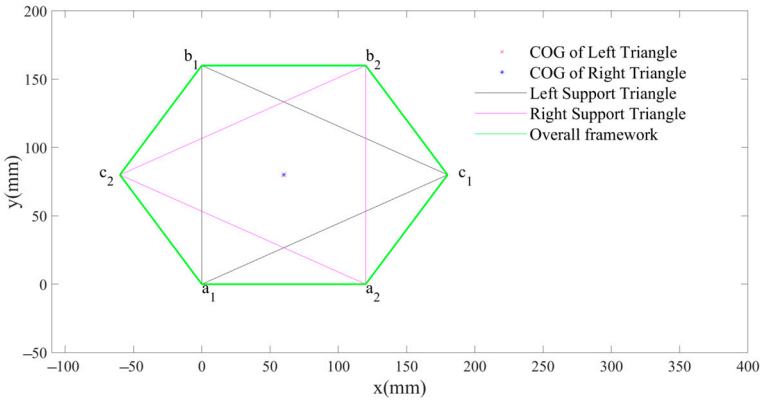
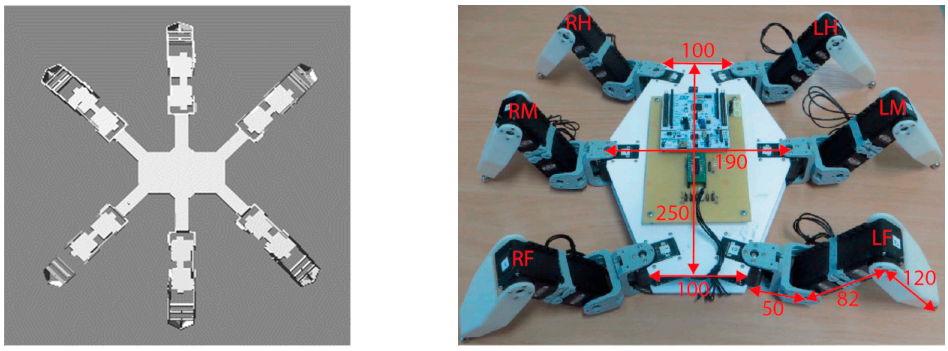



**Figure 17.** Analysis of MATLAB.

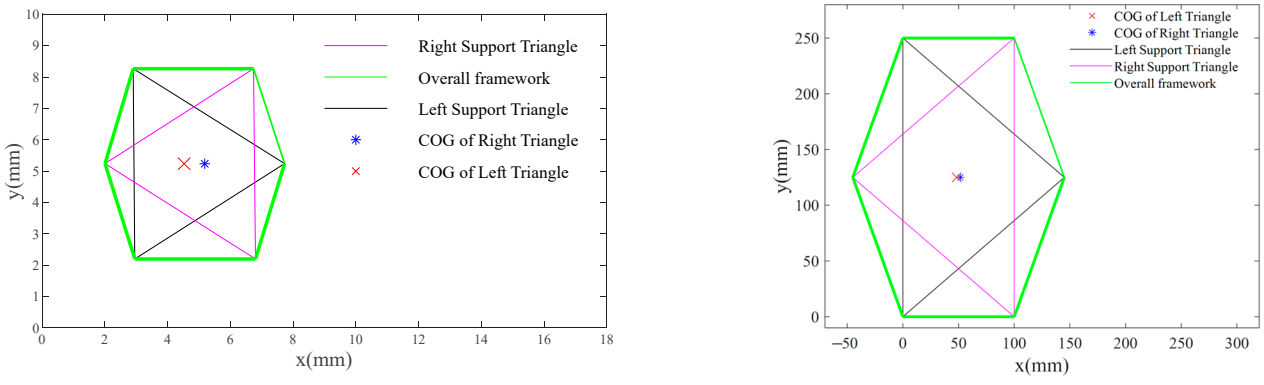
Two kinds of bionic spider robots with a convex hexagonal layout are selected, as documented in Figure 18.




(**a**) (**b**)

**Figure 18.** Comparison object: (**a**) sketch of the overall structure of the lunar exploration hexapod robot [44]; (**b**) hexapod robot model HexaV4 [28].

Origin and MATLAB were used to extract, analyze, and process the data. The changes in the center of gravity were analyzed, as shown in Figure 19.




(**a**) (**b**)

**Figure 19.** Simulation result, (**a**) simulation result is performed for Figure 18a; (**b**) simulation result is performed for Figure 18b.

To analyze the shift in the center of gravity, a reference parameter, the center-of-gravity offset rate ($\rho$) is used, which is calculated as demonstrated in Equation (26).

$$\rho = (distance_{\mathrm{ab}})/(distance_{\mathrm{c}}) \quad (26)$$

In Equation (26), $distance_{ab}$ represents the distance between the center of gravity of the two supporting triangles in the triangular gait, while $distance_c$ denotes the inter-leg spacing on both sides of the triangular gait. The calculated center-of-gravity shift rates for all three are presented in Table 5.

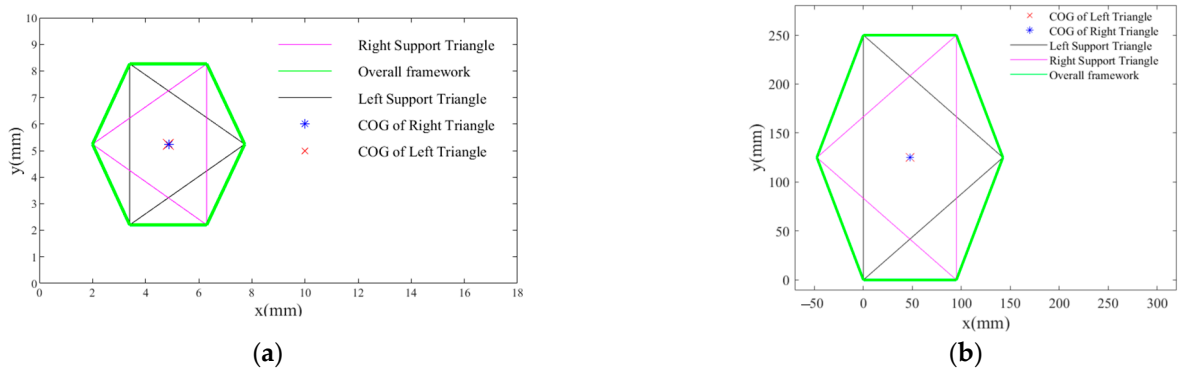
**Table 5.** Center-of-gravity deviation.

| Symbol | Paraphrase | Parameter Values (%) |
|---|---|---|
| $\rho_1$ | Our paper | 0 |
| $\rho_2$ | Article [44] | 11.4020 |
| $\rho_3$ | Article [28] | 1.7544 |

As indicated in Table 5, utilizing a program to regulate the stability of a robot requires a significant amount of computational space, which decreases the overall response rate, especially for Article [44]. By employing a center-of-gravity analysis method, the connecting points are redesigned.

Based on the above analysis, there are two methods to improve stability: (1) altering the distance between the connecting points of the front and back legs; (2) changing the distance between the connecting points of the middle leg.

Considering the overall configuration, and since the widest part of the robot occurs at the middle leg, we adjusted the distance between the connecting points of the front and back legs, as shown in Figure 20, to achieve 100% center-of-gravity coincidence during the transition between the two support phases. This enhancement can increase the stability of the robot during its movement.




(**a**) (**b**)

**Figure 20.** Optimization analysis, (**a**) optimization analysis is performed for Figure 19a; (**b**) optimization analysis is performed for Figure 19b.

### *4.2. Analysis of Leg*

#### 4.2.1. Trajectory Analysis

The mathematical model of the leg was established using MATLAB, and the motion trajectory of the foot, the slider and point D (knee joint) under ideal conditions and simulated actual operating conditions were analyzed.

Following the analysis of the leg design discussed in Section 3, kinematic simulations of the leg were performed using MATLAB software. The simulation conditions were set under static scenarios to investigate the leg's lifting and swinging movements, with the relevant parameters presented in Table 6.

During the leg operation, due to the arrangement angle, the movement rules of the front and rear four legs are similar, and the two middle legs are the same. Therefore, the second and sixth legs of the right triangle in Figure 10a are selected as examples. The operation time is 1 s, and a forward movement of 19 mm is completed. The x, y, and z changes in the relevant positions are plotted with the body coordinate system as a reference. The body frame data are shown in Table 4.

**Table 6.** Initial key parameter of leg.

| Symbol | Description | Parameter |
|---|---|---|
| $\theta_w$ | Swing range of *i*-th leg | $\pm 10^\circ$ |
| $\theta$ | Initial installation angle between the rod BC and the rod CD | $120^\circ$ |
| AB | $l_1$ | 50 mm |
| BC | $l_2$ | 100 mm |
| CD | $l_3$ | 100 mm |
| DE | $l_4$ | 150 mm |
| EG | $l_5$ | 30 mm |
| EF | $l_6$ | 400 mm |
| ∠BCD | $\theta$ | $120^\circ$ |

The speeds of the two motors are shown in Figure 21. From the analysis in Section 3.1, it can be seen that the selection requirements for the swing motor are relatively low, which is conducive to reducing the overall cost. The motor selected in the leg-lifting part can also avoid motors with special performance.

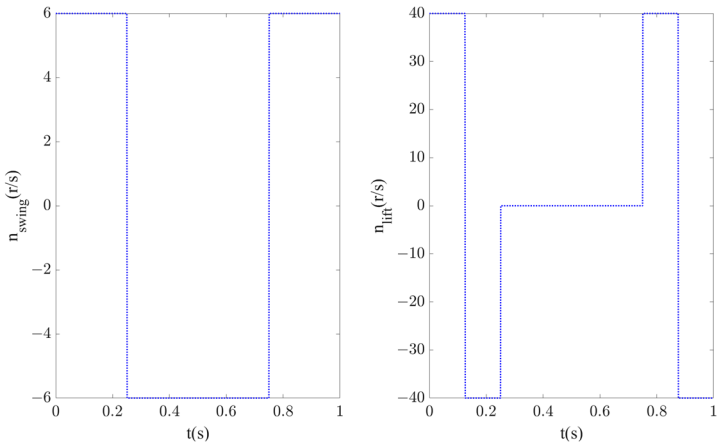



**Figure 21.** Motor speed.

As can be seen from Figure 22, the displacement trends of various components of the robot are similar during the movement. In (c) and (f), the z coordinate displacement changes slowly from the beginning to end. At this time, the legs are in the state of lifting or lowering, and need to overcome the resistance from the ground. When they are not in contact with the ground, the remaining movements can be completed quickly to reduce the movement loss time.

In (b) and (e), the movement trajectories of legs two and six are similar, and their peak or valley values appear when the legs are lifted at the maximum angle, respectively. Due to their lifting and lowering, the change in this coordinate is formed. In the middle, that is, 0.25–0.75 s, since the body is used as the reference coordinate system during the forward process, the legs move backward relative to the body during this time period, meaning that the y coordinate decreases.

In (a) and (d), relative displacement occurs when in the support phase, which corresponds to the analysis of the triangular gait in Section 2.2.2. The overall movement trajectory presents a zigzag shape and corresponds to Figure 2.

As seen in Figure 23, the speed of lifting and lowering the legs is balanced, which avoids large torque impacts on various components, improves the operating stability of the mechanism, and reduces the control cost of the motor.

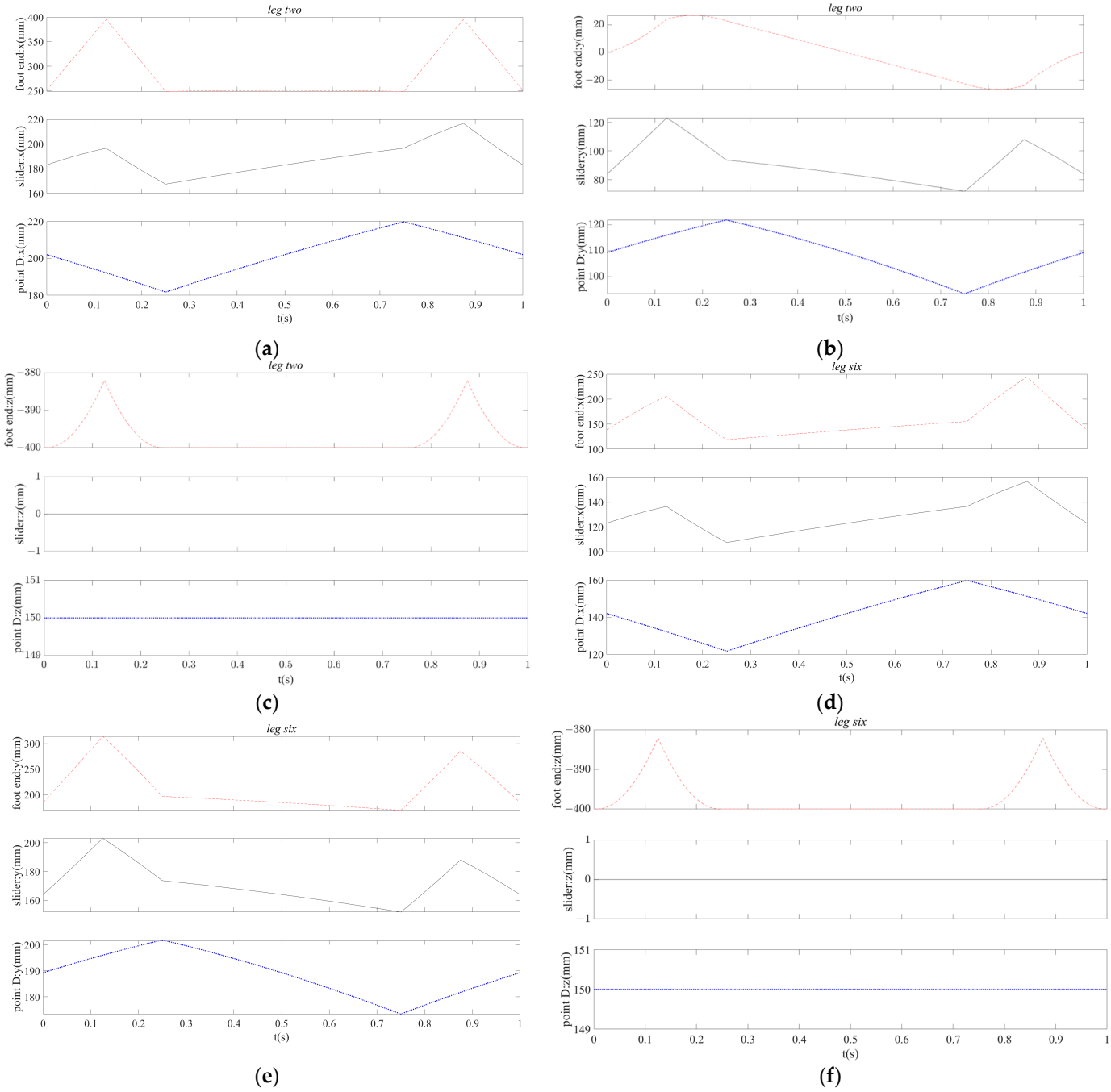



**Figure 22.** (**a**) The motion trajectory of the foot of the leg two; (**b**) the movement locus of the slider of the leg two; (**c**) the movement locus of the slider of the leg two; (**d**) the motion trajectory of the foot of the leg six; (**e**) the movement locus of the slider of the leg six; (**f**) the movement locus of the slider of the leg six.

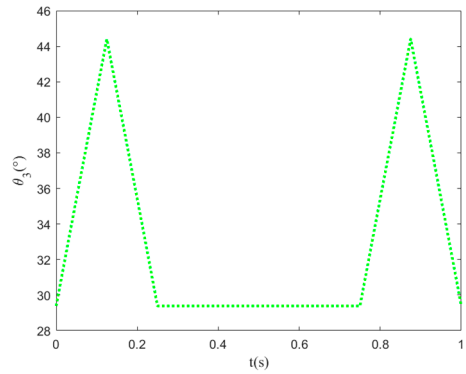
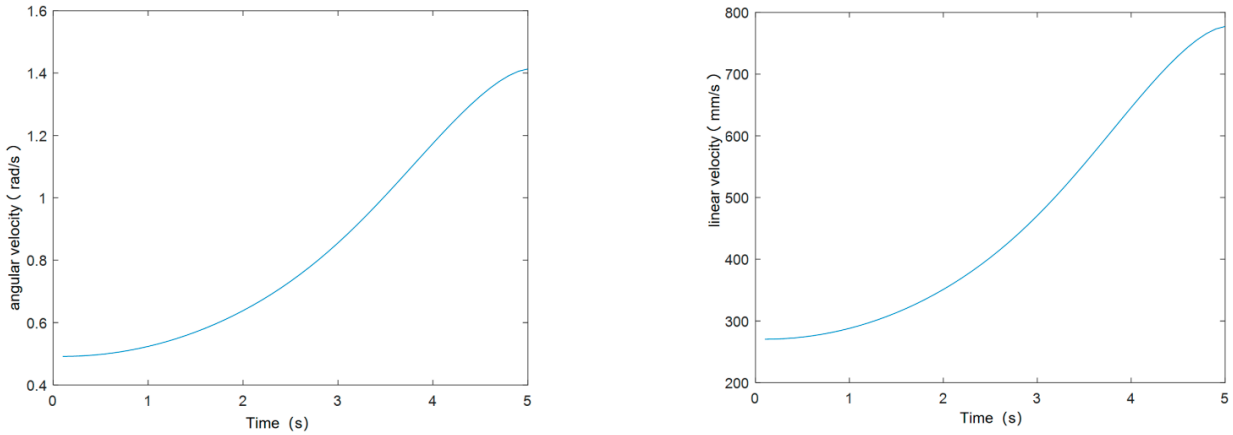



**Figure 23.** Variation in the leg-lifting angle.

#### 4.2.2. Simulation Analysis

The actual operation of the motor is analyzed. When the motor starts and stops, it will produce a very short acceleration and deceleration stage. We slow down the leg-lifting action so that it is completed within 5 s. The angular velocity and linear velocity of the foot end when the leg is lifted are analyzed. As depicted in Figure 24, the speed is in the slow change stage in the start and stop stages, but the time it occupies is relatively short. It can be seen that in the actual operation process, the impact of this part on the operation of the mechanism can be ignored. The changes in angular velocity and linear velocity are from slow to fast, which can help the legs overcome the resistance of the external environment.




(**a**) (**b**)

**Figure 24.** (**a**) Angular velocity of $\theta_3$; (**b**) linear velocity of the motion trajectory of the foot.

In summary, the movement pattern of the leg joint is restored by the linkage group, and a unified driving joint is adopted to achieve the bending of the leg with a single power source. The entire mechanism consists of a two-degree-of-freedom motion mechanism composed of a linkage mechanism, which meets the operational requirements of the leg with a low delay response and reduced complexity of control algorithms, thereby reducing the control cost of the biomimetic spider robot. Furthermore, with the reduction in the number of drive sources, the manufacturing cost of the leg is also reduced, and the waterproofing cost in humid environments is decreased, thereby reducing the likelihood of damage. Moreover, with the structural change, the motor power is transmitted through the transmission mechanism to achieve leg movement, which maximally reduces direct motor loading, allowing the motor's output efficiency to be fully applied to the leg's movement, avoiding unnecessary energy consumption. This reduction also lowers the size and cost of the power source carried by the robot, facilitating low-cost popularization of the robot. When a component of the leg fails, modular replacement is convenient, as the connecting

pins and installation components can be separated to complete the disassembly without rewiring, which improves the maintenance efficiency of the robot in specific situations and reduces time losses.

#### 4.2.3. Uncertainty Analysis

We partially adjusted the length of each part of the leg to analyze its impact on the movement trajectory. We used the variable analysis method to analyze the foot end trajectory.

The values of EG were changed, as seen in Figure 25.

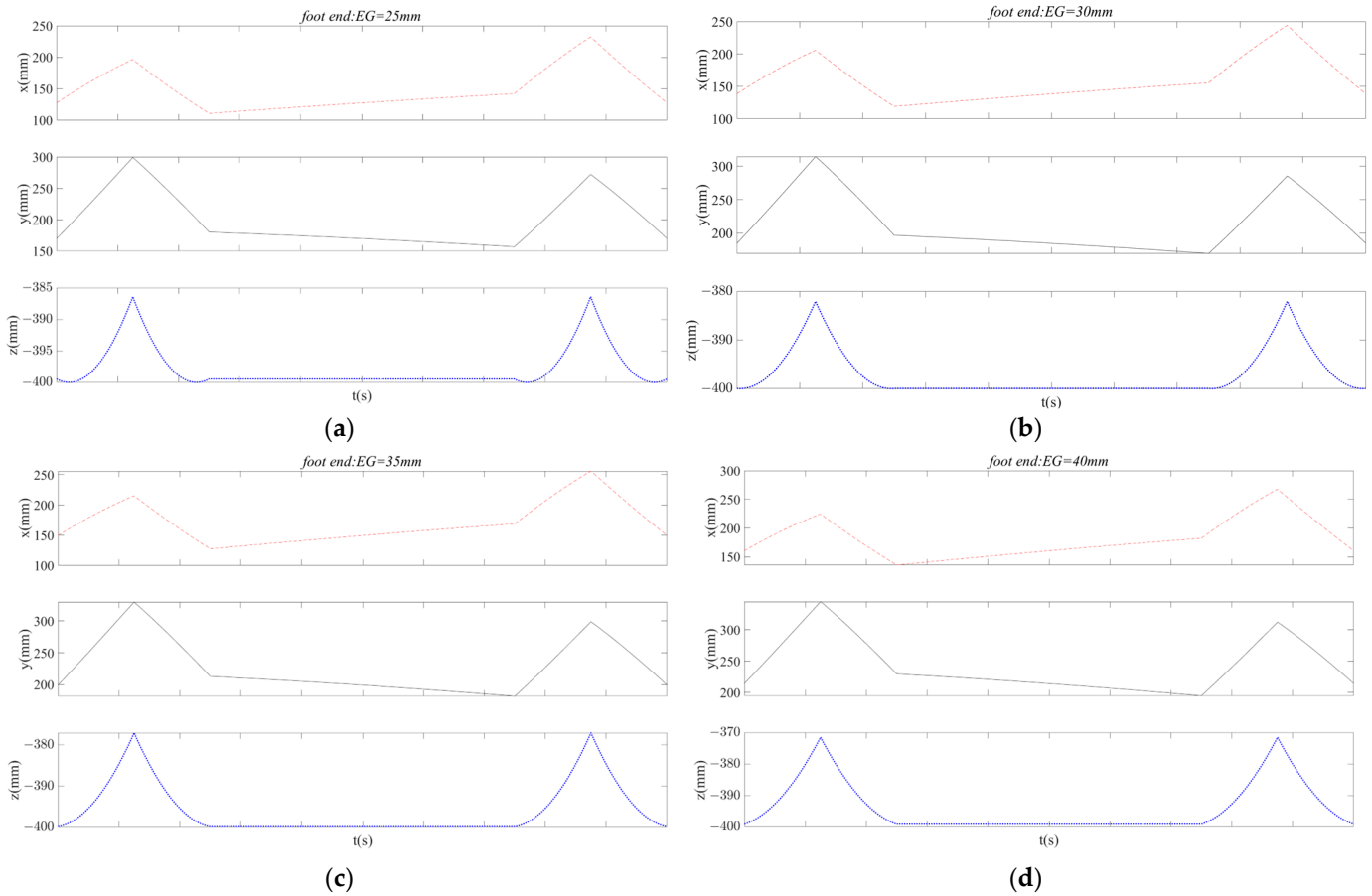



**Figure 25.** Foot trajectory during EG changes, (**a**) EG = 25; (**b**) EG = 30; (**c**) EG = 35, (**d**) EG = 40.

In Figure 25, when EG is 25 mm, although its peak change trend is faster, it will form a lower height than the initial height when lifted, causing deep friction between the legs and the ground, which is not conducive to the rapid lifting of the legs. Increasing this parameter will cause the movement speed of the foot to slow down. Therefore, the change in this parameter will affect the movement speed of the foot and the lifting height.

As can be seen in the Figure 26, the change in DE has a small impact on the x and y directions, but a large impact on the z direction. As DE increases, the overall ground clearance of the robot increases, but at 135 mm and 165 mm, it is obvious that the z coordinate of the foot end during operation is smaller than the z coordinate in the static state; that is, if it is in actual operation, the leg will lift the entire robot and move, which will consume more energy. Therefore, it is not advisable. Among these five parameters, 150 mm is the best connection, so it is the final value selected for this simulation.

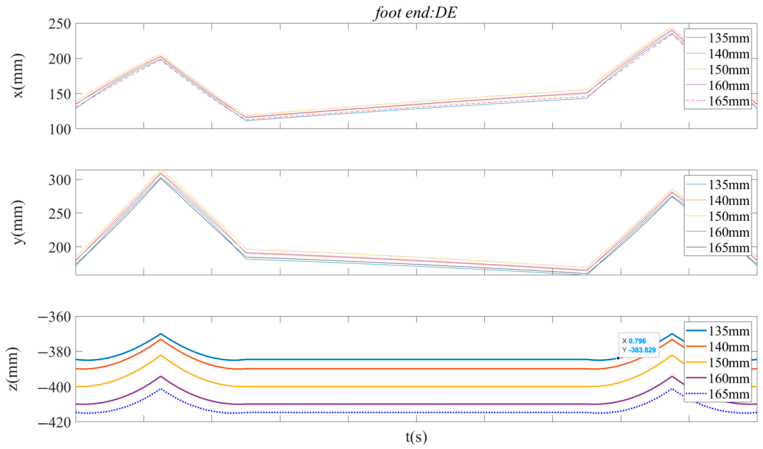



**Figure 26.** Foot trajectory during DE changes.

#### 4.2.4. Comparative Analysis

We selected the bionic spider robots in recent years for comparison, as shown in Table 7.

**Table 7.** Comparative analysis.

| Criteria | Sketch of the Overall Structure of the Lunar Exploration Hexapod Robot [44] | Hexapod Robot Model HexaV4 [28] | Two-DOF Design (Our Study) |
|---|---|---|---|
| Control Complexity | High, requiring advanced gait optimization algorithms. | High, requiring heuristic algorithms for gait switching. | Low, with simplified control architecture using a multi-link mechanism. |
| Energy Consumption | Optimized for stability and energy efficiency using an improved triangular gait. | Reduced through heuristic gait switching. | Lowered through a simplified design and dual-motor system. |
| Maintenance Costs | Moderate, due to complexity in gait optimization systems. | Moderate to high, depending on the complexity of heuristic control systems. | Low, with fewer moving parts and a simpler design. |

### *4.3. Initial Verification*

In this study, we developed a biomimetic spider robot prototype using the Fisher Technik system, as shown in Figure 27, which validated our proposed new leg design with two degrees of freedom and hexagonal body structure. The two-degree-of-freedom leg structure combines a multi-link mechanism and a dual-motor system, enhancing the control of leg movement and improving leg strength. The hexagonal body structure and triangular gait were carefully designed to align weight with support points, thereby enhancing stability.

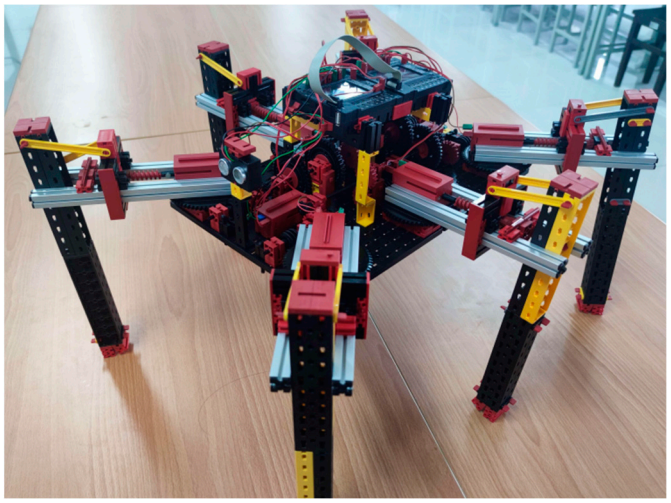


**Figure 27.** A biomimetic spider robot prototype using the Fisher Technik system.

### *4.4. Summary*

Through the above analysis, it is evident that during the design process of a hexapod robot's body, the connection points between the legs and the body are crucial for the robot's ability to move quickly and stably. A well-designed connection point can ensure that the robot's legs are subjected to uniform forces, thereby reducing the wear rate of each leg. It is observed that, under the condition of equal width, the choice of a convex hexagonal structure better meets the requirements for center-of-gravity distribution. For the analysis of the legs, the movement characteristics meet the requirements of robot walking.

## 5. Conclusions

This paper explores the theoretical elements of the structural design of a biomimetic spider robot, specifically focusing on its leg configuration and body structure. The robot obtains enhanced mobility and flexibility by employing a composite linkage system and altering its leg structure, resulting in a two-degree-of-freedom design. The body structure of the robot is designed in a convex hexagon shape, which is inspired by the analysis of spider movement, in order to replicate all-terrain capabilities. The biomimetic technique streamlines the leg structure by utilizing a dual-motor system. This not only reduces the complexity of the robot, but also enhances the stability of the control system, while increasing the speed of the reaction.

In addition, the D-H parameter method was used to carry out static analysis, which effectively verified the final operating state of the robot, including not only the speed during operation, but also the angular velocity. Through analysis, it is proved that it can react quickly and has the ability to navigate obstacles. These capabilities are indispensable to ensure its trafficability characteristic in complex environments. For the body structure, the total center of gravity of the robot is considered in order to ensure that the robot has the optimal framework of stability. The convex hexagonal structure can realize the same position coordinates of the two sets of center of gravity, so as to ensure the continuous stability of the robot during its operation. After this theoretical analysis, we will use the existing model to complete the structural analysis according to the actual working conditions, conduct physical prototype trials, improve the relevant control algorithms, complete the actual operation test, and further optimize the control and structure.

**Author Contributions:** Methodology, Y.N., D.Z., Y.C. and L.W.; software, Y.N., D.Z. and Y.C.; validation, Y.N., D.Z. and Y.C.; formal analysis, Y.N. and D.Z.; investigation, Y.N. and Y.C.; writing—original draft preparation, D.Z. and Y.C.; writing—review and editing, X.H. All authors have read and agreed to the published version of the manuscript.

**Funding:** This research was funded by the 2023 National Innovation and Entrepreneurship Academy Construction Project at Xi'an University of Architecture and Technology'Design and Practice of Scientific and Technological Works Based on Fischertechnik Robot' (Grant No. XAUATC2023-05KCJS-01); Shaanxi Natural Science Foundation General Program (Grant No. 2023-JC-YB-294).

**Institutional Review Board Statement:** Not applicable.

**Informed Consent Statement:** Not applicable.

**Data Availability Statement:** The data presented in this study are available upon request from the corresponding author.

**Conflicts of Interest:** The authors declare no conflicts of interest.

## References

1. Li, Z.; Song, Y.; Zhang, X.; Peng, X.; Xu, N. Modeling of Walking-Gait Parameters and Walking Strategy for Quadruped Robots. *Appl. Sci.* **2023**, *13*, 6876. [CrossRef]
2. Chatziparaschis, D.; Lagoudakis, M.G.; Partsinevelos, P. Aerial and ground robot collaboration for autonomous mapping in search and rescue missions. *Drones* **2020**, *4*, 79. [CrossRef]
3. Lee, C.H.; Kim, S.H.; Kang, S.C.; Kim, M.S.; Kwak, Y.K. Double-track mobile robot for hazardous environment applications. *Adv. Robot.* **2003**, *17*, 447–459. [CrossRef]
4. Zhang, D.; Pan, G.; Cao, Y.; Huang, Q.; Cao, Y. Engineering A novel integrated gliding and flapping propulsion biomimetic manta-ray robot. *J. Mar. Sci. Eng* **2022**, *10*, 924. [CrossRef]
5. Shi, Q.; Gao, J.; Wang, S.; Quan, X.; Jia, G.; Huang, Q.; Fukuda, T. Development of a small-sized quadruped robotic rat capable of multimodal motions. *IEEE Trans. Robot.* **2022**, *38*, 3027–3043. [CrossRef]
6. Wang, C.; Wang, S.; Ma, H.; Zhang, H.; Xue, X.; Tian, H.; Zhang, L. Research on the Obstacle-Avoidance Steering Control Strategy of Tracked Inspection Robots. *Appl. Sci.* **2022**, *12*, 10526. [CrossRef]
7. Ab Rashid, M.Z.; Yakub, M.F.M.; bin Shaikh Salim, S.A.Z.; Mamat, N.; Putra, S.M.S.M.; Roslan, S.A. Modeling of the in-pipe inspection robot: A comprehensive review. *Ocean. Eng.* **2020**, *203*, 107206. [CrossRef]
8. Rusu, C.; Tatar, M.O. Adapting Mechanisms for In-Pipe Inspection Robots: A Review. *Appl. Sci.* **2022**, *12*, 6191. [CrossRef]
9. Zhang, X.; Pan, T.; Heung, H.L.; Chiu, P.W.Y.; Li, Z. A biomimetic soft robot for inspecting pipeline with significant diameter variation. In Proceedings of the 2018 IEEE/RSJ International Conference on Intelligent Robots and Systems (IROS), Madrid, Spain, 1–5 October 2018.
10. Jeong, Y.C.; Kang, K. A monolithic sandwich panel for insect-mimicking micro drones. *Mater. Des.* **2020**, *187*, 108376. [CrossRef]
11. Lan, Z.; Jiang, S.J. Design and simulation of the biomimetic flexible fish fin propeller on submarine. *Adv. Mater. Res.* **2014**, *1006*, 223–226. [CrossRef]
12. Pan, X.; Wang, Q.; He, P.; Liu, K.; Ni, Y.; Chen, L.; Ouyang, X.; Huang, L.; Wang, H.; Xu, S. A bionic tactile plastic hydrogel-based electronic skin constructed by a nerve-like nanonetwork combining stretchable, compliant, and self-healing properties. *Chem. Eng. J.* **2020**, *379*, 122271. [CrossRef]
13. Miao, Y.; Xu, M.; Yu, J.; Zhang, L.J. Conductive cold-resistant and elastic hydrogel: A potential bionic skin for human-machine interaction control over artificial limbs. *Sens. Actuators B Chemical* **2021**, *327*, 128916. [CrossRef]
14. Shi, J.; Zhu, L.; Li, L.; Li, Z.; Yang, J.; Wang, X. A TPMS-based method for modeling porous scaffolds for bionic bone tissue engineering. *Sci. Rep.* **2018**, *8*, 7395. [CrossRef] [PubMed]
15. Du, H.; Li, G.; Sun, J.; Zhang, Y.; Bai, Y.; Qian, C.; Liang, Y. Structures A review of shape memory alloy artificial muscles in bionic applications. *Smart Mater. Struct.* **2023**, *32*, 103001. [CrossRef]
16. Wang, Y.L.; Wang, K.Y.; Wang, K.C.; Mo, Z.J. Safety evaluation and experimental study of a new bionic muscle cable-driven lower limb rehabilitation robot. *Sensors* **2020**, *20*, 7020. [CrossRef]
17. Linares, J.C.; Barrientos, A.; Márquez, E.M. Hybrid bio-inspired architecture for walking robots through central pattern generators using open source fpgas. In Proceedings of the 2018 IEEE/RSJ International Conference on Intelligent Robots and Systems (IROS), Madrid, Spain, 1–5 October 2018.
18. Shumilov, V.; Syryamkin, V.; Syryamkin, M. Modelling of pathologies of the nervous system by the example of computational and electronic models of elementary nervous systems. *AIP Conf. Proc.* **2015**, *1688*, 040007.
19. Kano, T.; Ishiguro, A.J. Decoding decentralized control mechanism underlying adaptive and versatile locomotion of snakes. *Integr. Comp. Biol.* **2020**, *60*, 232–247. [CrossRef]
20. Marinoni, A.; Bono, F. Modelling and Control of a Quadruped-Spider Robot: Simulation and Scale Prototype Implementation. Master's Thesis, Politecnico di Milano, Milan, Italy, 2022.
21. Kravchenko, V.V.; Efremov, A.A.; Zhilenkov, A.A.; Kozlov, V.N.; Kristina, G.; Anton, P.; Mark, P.; Mikhail, S.J. Control Mathematical model of a robot-spider for group control synthesis: Derivation and validation. *JRC* **2023**, *4*, 849–855. [CrossRef]
22. Zhu, Y.; Chen, L.; Liu, Q.; Qin, R.; Jin, B. Omnidirectional jump of a legged robot based on the behavior mechanism of a jumping spider. *Appl. Sci.* **2018**, *8*, 51. [CrossRef]

23. Sun, C.; Yuan, M.; Li, F.; Yang, Z.; Ding, X. Design and simulation analysis of hexapod bionic spider robot. *J. Phys. Conf. Ser.* **2019**, *1168*, 022094. [CrossRef]
24. Liu, C.; Chen, S.; Sheng, C.; Ding, P.; Qian, Z.; Ren, L.J. The art of a hydraulic joint in a spider's leg: Modelling, computational fluid dynamics (CFD) simulation, and bio-inspired design. *J. Comp. Physiol. A* **2019**, *205*, 491–504. [CrossRef] [PubMed]
25. Wu, M.; Song, C.; Zhang, W. Design and Analysis of Spider-Like Robot Control System. In Proceedings of the International Conference on Maintenance Engineering, Zhuhai, China, 23–25 October 2020.
26. Jiang, X.; Yang, J.; Zeng, L.; Huang, C. A Spider-Joint-like Bionic Actuator with an Approximately Triangular Prism Shape. *Biomimetics* **2023**, *8*, 299. [CrossRef] [PubMed]
27. Fang, G.; Cheng, J. Advances in climbing robots for vertical structures in the past decade: A review. *Biomimetics* **2023**, *8*, 47. [CrossRef] [PubMed]
28. Luneckas, M.; Luneckas, T.; Kriaučiūnas, J.; Udris, D.; Plonis, D.; Damaševičius, R.; Maskeliūnas, R. Hexapod Robot Gait Switching for Energy Consumption and Cost of Transport Management Using Heuristic Algorithms. *Appl. Sci.* **2021**, *11*, 1339. [CrossRef]
29. Baatrup, E.; Bayley, M.J. Quantitative analysis of spider locomotion employing computer-automated video tracking. *Physiol. Behav.* **1993**, *54*, 83–90. [CrossRef]
30. Hao, X.; Ma, W.; Liu, C.; Li, Y.; Qian, Z.; Ren, L.; Ren, L. Analysis of spiders' joint kinematics and driving modes under different ground conditions. *Appl. Bionics Biomech.* **2019**, *2019*, 4617212. [CrossRef]
31. Wang, Z.; Wang, J.; Ji, A.; Li, H.; Dai, Z. Movement behavior of a spider on a horizontal surface. *Chin. Sci. Bull.* **2011**, *56*, 2748–2757. [CrossRef]
32. Wolff, J.O. Locomotion and kinematics of arachnids. *J. Comp. Physiol. A* **2021**, *207*, 99–103. [CrossRef]
33. Biancardi, C.M.; Fabrica, C.G.; Polero, P.; Loss, J.F.; Minetti, A.E. Biomechanics of octopedal locomotion: Kinematic and kinetic analysis of the spider *Grammostola mollicoma*. *J. Exp. Biol* **2011**, *214*, 3433–3442. [CrossRef]
34. Landkammer, S.; Winter, F.; Schneider, D.; Hornfeck, R. Biomimetic spider leg joints: A review from biomechanical research to compliant robotic actuators. *Robotics* **2016**, *5*, 15. [CrossRef]
35. Suter, R.B.; Stratton, G.; Miller, P.R. Water surface locomotion by spiders: Distinct gaits in diverse families. *J. Arachnol.* **2003**, 428–432. [CrossRef]
36. Spagna, J.C.; Valdivia, E.A.; Mohan, V.J. Gait characteristics of two fast-running spider species (*Hololena adnexa* and *Hololena curta*), including an aerial phase (Araneae: Agelenidae). *J. Arachnol.* **2011**, *39*, 84–91. [CrossRef]
37. Grabowska, M.; Godlewska, E.; Schmidt, J.; Daun-Gruhn, S.J. Quadrupedal gaits in hexapod animals–inter-leg coordination in free-walking adult stick insects. *J. Exp. Biol* **2012**, *215*, 4255–4266. [CrossRef] [PubMed]
38. Guo, S.; Gao, S.; Chen, T.; Li, Y.; Wang, Y.; Zheng, L.; Zhang, C. Structural Design and Analysis of Biomimetic Rescue Spider Robot. In Proceedings of the 2024 3rd International Symposium on Control Engineering and Robotics, Changsha, China, 24–26 May 2024.
39. Bender, J.A.; Simpson, E.M.; Tietz, B.R.; Daltorio, K.A.; Quinn, R.D.; Ritzmann, R.E. Kinematic and behavioral evidence for a distinction between trotting and ambling gaits in the cockroach *Blaberus discoidalis*. *J. Exp. Biol* **2011**, *214*, 2057–2064. [CrossRef] [PubMed]
40. Kyberd, P.J.; Holland, O.E.; Chappell, P.H.; Smith, S.; Tregidgo, R.; Bagwell, P.J.; Snaith, M.J. MARCUS: A two degree of freedom hand prosthesis with hierarchical grip control. *IEEE Trans. Rehabil. Eng* **1995**, *3*, 70–76. [CrossRef]
41. Umeno, T.; Hori, Y.J. Robust speed control of DC servomotors using modern two degrees-of-freedom controller design. *IEEE Trans. Ind. Electron* **1991**, *38*, 363–368. [CrossRef]
42. Maalouf, D.; Moog, C.H.; Aoustin, Y.; Li, S. Applications Classification of two-degree-of-freedom underactuated mechanical systems. *IET Control. Theory Appl.* **2015**, *9*, 1501–1510. [CrossRef]
43. Norton, R.L. *Machine Design*; Prentice Hall: London, UK, 2010.
44. Guo, Y.-Q.; Luo, W.-H.; Xu, Z.-D.; Shu, B.-M.; Yang, D.-K. Research on the Design and Gait Planning of a Hexapod Robot Based on Improved Triangular Gait for Lunar Exploration. *Appl. Sci.* **2023**, *14*, 260. [CrossRef]
45. Zhang, Y.; Qiao, G.; Wan, Q.; Tian, L.; Liu, D. A novel double-layered central pattern generator-based motion controller for the hexapod robot. *Mathematics* **2023**, *11*, 617. [CrossRef]
46. Ni, Y.; Li, L.; Qiu, J.; Sun, Y.; Qin, G.; Han, Q.; Ji, A. A Novel Wheel-Legged Hexapod Robot. *Biomimetics* **2022**, *7*, 146. [CrossRef]
47. Liu, Y.; Fan, X.; Ding, L.; Wang, J.; Liu, T.; Gao, H. Fault-tolerant tripod gait planning and verification of a hexapod robot. *Appl. Sci.* **2020**, *10*, 2959. [CrossRef]


**Disclaimer/Publisher's Note:** The statements, opinions and data contained in all publications are solely those of the individual author(s) and contributor(s) and not of MDPI and/or the editor(s). MDPI and/or the editor(s) disclaim responsibility for any injury to people or property resulting from any ideas, methods, instructions or products referred to in the content.